DTU Library

The enhanced X-ray Timing and Polarimetry mission – eXTP
an update on its scientific cases, mission profile and development status

Zhang, Shuang Nan; Santangelo, Andrea; Xu, Yupeng; Feroci, Marco; Hernanz, Margarita; Lu, Fangjun; Chen, Yong; Feng, Hua; Nandra, Kirpal; Jiang, Weichun

Total number of authors:
347

[Link back to DTU Orbit](#)

The enhanced X-ray Timing and Polarimetry mission – eXTP: an update on its scientific cases, mission profile and development status

Shuang-Nan Zhang[1], Andrea Santangelo[2], Yupeng Xu[1], Marco Feroci[3,4], Margarita Hernanz[5,6], Fangjun Lu[1], Yong Chen[1], Hua Feng[7], Kirpal Nandra[8], Weichun Jiang[1], Jiri Svoboda[9], Søren Brandt[10], Stéphane Schanne[11], Jean in 't Zand[12], Malgorzata Michalska[13], Enrico Bozzo[14], Emrah Kalemci[15], Ivan Agudo[16], Mahdi Ahangarianabhari[17], Gabby Aitink-Kroes[12], Giovanni Ambrosi[18], Filippo Ambrosino[3], Zhenghua An[1], Miguel Angel Perez Torres[16], Matias Antonelli[19], Andrea Argan[3,20], Viktor Babinec[21], Luca Baldini[22], Marco Barbera[23,24], Coen van Baren[12], David Baudin[11], Jörg Bayer[2], Ronaldo Bellazzini[22], Pierluigi Bellutti[25], Bruna Bertucci[26], Giuseppe Bertuccio[17], Xingzi Bi[27], Mirko Boezio[19], Valter Bonvicini[19], Walter Bonvicini[19], Pol Bordas[28], Alice Borghese[5,6], Giacomo Borghi[25], Florent Bouyjou[11], Ayhan Bozkurt[15], Alessandro Brez[22], Daniele Brienza[29], Franck Cadoux[30], Riccardo Campana[31], Jiewei Cao[1], Xuelei Cao[1], Jorge Casares[32], Elisabetta Cavazzuti[29], Francesco Ceraudo[3], Tianxiang Chen[1], Wen Chen[27], Can Chen[1], Yupeng Chen[1], Xin Chen[27], Yehai Chen[27], Jerome Chenevez[10], Yaodong Cheng[1], Daniela Cirrincione[33,19], Marta Civitani[34], Min Cong[1], Francesco Coti Zelati[5,6], Weiwei Cui[1], Tao Cui[1], Wei Cui[7], Boyu Dai[1], Thomas Dauser[35], Nicolas De Angelis[30], Barbara De Marco[36], Alessandra De Rosa[3], Ettore Del Monte[3,4], Sergio Di Cosimo[3], Sebastian Diebold[2], Giuseppe Dilillo[3], Fei Ding[37], Roman Dohnal[21], Zefang Dong[1], Immacolata Donnarumma[29], Michal Dovciak[9], Yuanyuan Du[1], Lorenzo Ducci[2], Yuri Evangelista[3,4], Qingmei Fan[38], Yannick Favre[30], Patrícia Ferrés[5,6], Emanuele Fiandrini[26], Francesco Ficorella[25], Fabio Fuschino[31], José Luis Gálvez[5,6], Na Gao[1], Min Gao[1], Yuqiang Ge[37], Mingyu Ge[1], Olivier Gevin[11], Marco Grassi[39], Yudong Gu[1], Quanying Gu[38], Ju Guan[1], Manuel Guedel[40], Xingbo Han[27], Dawei Han[1], Huilin He[1], Junwang He[27], Paul Hedderman[2], Jan-Willem den Herder[12], Bin Hong[38], Ander Hormaetxe[5,6], Dongjie Hou[1], Zexun Hu[41], Hao Hu[1], Qingbao Hu[1], Yu Hu[1], Yue Huang[1], Jiangjiang Huang[27], Qiushi Huang[42], Jia Huo[1], Richard Hynek[21], Kazumi Iwasawa[28], Lucca Izzo[16], Long Ji[43], Shumei Jia[1], Bowen Jiang[41], Wei Jiang[37], Jiechen Jiang[1], Xiaowei Jiang[1], Yang Jiao[1], Ge Jin[41], Fan Jin[37], Jordi Jose[36], Vladimir Karas[9], Thomas Kennedy[44], Christian Kirsch[35], Merlin Kole[30], Martin Komarek[21], Ingo Kreykenbohm[35], Lucien Kuiper[12], Irfan Kuvvetli[10], Claudio Labanti[31], Luca Latronico[45], Phillip Laubert[12], Tao Li[41], Longhui Li[41], Hong Li[7], Duo Li[37], Wei Li[1], Maoshun Li[1], Gang Li[1], Xiaobo Li[1], Chengkui Li[1], Bing Li[1], Haibo Li[1], Hong Liang[27], Qiuyan Liao[37], Jinyuan Liao[1], Olivier Limousin[11], Yanjian Lin[41], Manuel Linares[36], Rui Liu[27], Yichen Liu[46,47], Zhihao Liu[37], Hongwei Liu[1], Xiaojing Liu[1], Xiaohua Liu[1], Ugo Lo Cicero[24], Jens Loehring[48], Giovanni Lombardi[3], Maximilian Lorenz[35], Bing Lu[1], Leonardo Lucchesi[22], Tao Luo[1], Laidan Luo[1], Jia Ma[1], Xiang Ma[1], Daniele Macera[17], Piero Malcovati[39], Alberto Manfreda[22], Josep Maria Paredes[28], Andrea Marinucci[29], Adrian Martindale[49], Norbert Meidinger[8], Filippo Mele[17], Vasco Mendes[50], Bin Meng[1], Martin Merkl[21], Aline Meuris[11], Giovanni Miniutti[51], Massimo Minuti[22], Alfredo Morbidini[3], Gianluca Morgante[31], Fabio Muleri[3,4], Riccardo Munini[19], Lorenzo Mussolin[26], Barbara Negri[29], Jianyin Nie[1], Petr Novák[52], Witold Nowosielski[13], Alessio Nuti[3], Ahmet Onat[53], Piotr Orleanski[13], Leonardo Orsini[22], Roland Ottensamer[40], Ge Ou[1], Luigi Pacciani[3], Stephane Paltani[14], Teng Pan[38], Kai Pan[41], Giovanni Pareschi[34], Alessandro Patruno[5,6], Giancarlo Pepponi[25], Emanuele Perinati[2], Raffaele Piazzolla[29], Antonino

Picciotto[25], Claudio Piemonte[25], Michele Pinchera[22], Samuel Pliego[2], Juri Poutanen[54,55], Liqiang Qi[1], Fazhi Qi[1], Pengfei Qiang[56], Fangjian Qiao[41], Zheng Qiao[37], Xiangbiao Qiu[41], Chengbo Qiu[27], Jinlu Qu[1], Alexandre Rachevski[19], Irina Rashevskaia[57], Nanda Rea[5,6], Marc Ribo[28], Rob de la Rie[12], Jerome Rodriguez[11], Pablo Rodríguez Gil[32], Gloria Sala[36], Thomas Schanz[2], Roberto Serafinelli[3], Carmelo Sgro[22], Zhengxiang Shen[42], Lizhi Sheng[56], Jingyan Shi[1], Giorgia Sironi[34], Konrad Skup[13], Liming Song[1], Zeyu Song[1], Jiangbo Song[38], Gloria Spandre[22], Daniele Spiga[34], Yongquan Su[46,58,47], Liang Sun[1], Müberra Sungur[59], Libor Švéda[9], Gianpiero Tagliaferri[34], Ying Tan[1], Lian Tao[1], Denis Tcherniak[10], Chris Tenzer[2], Michela Todaro[23,24], Laura Tolos[5,6], Gabriel Torok[60], Diego F. Torres[5,6], Alessio Trois[50], Onur Turhan[59], Phil Uttley[61], Andrea Vacchi[33,19], Enrico Virgilli[31], Channah Vogel[12], Dave Walton[44], Jian Wang[41], Xianqi Wang[2], Bo Wang[37], Langping Wang[62], Xiaofeng Wang[37], Dianlong Wang[63], Yusa Wang[1], Juan Wang[1], Hao Wang[1], Ruijie Wang[1], Ping Wang[1], Lingjun Wang[1], Wenshuai Wang[1], Tian Wang[27], Haoyu Wang[27], Zhanshan Wang[42], Anna L. Watts[61], Xiangyang Wen[1], Jörn Wilms[35], Berend Winter[44], Xin Wu[30], Chao Wu[41], Zhenyu Wu[46,58,47], Qiong Wu[7], Kaiji Wu[37], Hao Xiong[2], Shaolin Xiong[1], Wei Xu[41], Zhao Xu[41], Jingjing Xu[1], Xiongwei Xu[1], Jiadai Xue[37], Yongqing Yan[56], Xingtao Yan[56], Xianghui Yang[56], Yanji Yang[1], Xiongtao Yang[1], Sheng Yang[1], Jiawei Yang[1], Yingquan Yang[27], Shuxu Yi[1], Yonggao Yu[37], Ke Yu[1], Ganluigi Zampa[19], Nicola Zampa[19], Silvia Zane[44], Andrzej A. Zdziarski[64], Long Zhang[38], Shu Zhang[1], Wenda Zhang[9], Xiaoli Zhang[38], Zhen Zhang[41], Jiawei Zhang[41], Fan Zhang[1], Jiawei Zhang[1], Ziliang Zhang[1], Dali Zhang[1], Honglin Zhang[1], Aimei Zhang[1], Tong Zhang[1], Hongmei Zhang[1], Juan Zhang[1], Liang Zhang[1], Yueting Zhang[27], Li Zhao[37], Baosheng Zhao[56], Zijian Zhao[1], Xiaofan Zhao[1], Haisheng Zhao[1], Xiaoyun Zhao[1], Shijie Zheng[1], Yupeng Zhou[38], Xiaohong Zhou[56], Jiahuan Zhu[7], Yuxuan Zhu[1], Cheng Zhu[27], Zhencai Zhu[27], Nicola Zorzi[25], and Frans Zwart[12]

[1]Key Laboratory for Particle Astrophysics, Institute of High Energy Physics, CAS, Beijing 100049, China
[2]Institut für Astronomie und Astrophysik, Eberhard Karls Universität, Tübingen 72076, Germany
[3]INAF, Istituto di Astrofisica e Planetologia Spaziali, Via Fosso del Cavaliere 100, 00133 Rome, Italy
[4]INFN, Sezione Roma Tor Vergata, Via della Ricerca Scientifica, 00133, Rome, Italy
[5]Institute of Space Sciences (ICE-CSIC), Carrer de can Magrans, s/n, Campus UAB, 08193 Cerdanyola de Vallès (Barcelona), Spain
[6]Institut d'Estudis Espacials de Catalunya (IEEC), Barcelona, Spain
[7]Department of Engineering Physics and Center for Astrophysics, Tsinghua University, Beijing 100084, China
[8]Max Planck Institute for Extraterrestrial Physics, Giessenbachstr. 1, Garching 85748, Germany
[9]Astronomical Institute, Czech Academy of Sciences, Bocni II 1401, CZ-14100 Prague, Czech Republic
[10]DTU-Space, Technical University of Denmark, Lyngby, Denmark
[11]CEA Paris-Saclay, DRF/IRFU, 91191 Gif sur Yvette, France
[12]SRON Netherlands Institute for Space Research, NL-2333 CA Leiden, the Netherlands
[13]Space Research Center, Polish Academy of Sciences, Bartycka 18a, 00-716 Warszawa, Poland
[14]Department of Astronomy, University of Geneva, Chemin d'Ecogia 16, 1290, Versoix,

Switzerland

[15]Sabanci University, Faculty of Engineering and Natural Sciences, 34956, Istanbul, Turkey

[16]Instituto de Astrofysíca de Andalucia - CSIC, Granada 18008, Spain

[17]Politecnico di Milano, Polo di Como, Via Anzani 41, Como, Italy

[18]INFN, Sezione di Perugia, Via Alessandro Pascoli, 23c, 06123, Perugia, Italy

[19]INFN, Sezione di Trieste, Padriciano 99, 34149, Italy

[20]INAF, Viale del Parco Mellini 84, I-00136 Rome, Italy

[21]L.K. Engineering, s.r.o. Vídenská 55 63900 Brno Czech Republic

[22]Sezione di Pisa, Istituto Nazionale di Fisica Nucleare, Largo Bruno Pontecorvo, 3, Pisa 56127, Italy

[23]Università di Palermo, Dipartimento di Fisica e Chmica, Via Archirafi 36, 90123, Palermo, Italy

[24]INAF, Osservatorio Astronomico di Palermo, Piazza del Parlamento, 1, 90134, Palermo, Italy

[25]Fondazione Bruno Kessler, Via Sommarive, Povo, 38123, Trento, Italy

[26]University of Perugia, Dip. Fisica e Geologia, Via Pascoli snc - 06123 - Perugia Italy

[27]Innovation Academy for Microsatellites of CAS, Xueyang Road No.1, Pudong district, Shanghai, China

[28]ICREA & Institut de Cíencies del Cosmos (ICCUB), Universitat de Barcelona (IEEC-UB), Barcelona 08028, Spain

[29]Italian Space Agency, Via del Politecnico snc, 00133 Rome, Italy

[30]Department of Nuclear and Particle Physics, University of Geneva, CH-1205, Switzerland

[31]INAF, Osservatorio di astrofisica e scienza dello spazio di Bologna, Via P. Gobetti 101, Bologna, Italy

[32]Instituto de Astrofísica de Canarias, Tenerife 38205, Spain

[33]University of Udine, Via delle Scienze, 206, 33100, Udine, Italy

[34]Osservatorio Astronomico di Brera, Istituto Nazionale di Astofisica, Via Brera, 28, Milano 20121, Italy

[35]Remeis-Sternwarte & ECAP, Friedrich-Alexander-Universität Erlangen-Nürnberg, Sternwartstr. 7, 96049 Bamberg, Germany

[36]Universitat Politecnica de Catalunya (UPC-IEEC), Barcelona 08034, Spain

[37]Center for Precision Engineering, Harbin Institute of Technology, Harbin 150001, China

[38]Beijing Institute of Spacecraft System Engineering, CAST, Beijing 10094, China

[39]University of Pavia, Department of Electrical, Computer, and Biomedical Engineering, Via Ferrata 5, 27100 Pavia, Italy

[40]Universität Wien, Universitätsring 1, 1010 Wien, Austria

[41]North Night Vision Technology Co. Ltd, Nanjing 211106, China

[42]Key Laboratory of Advanced Material Microstructure of Education Ministry of China, Institute of Precision Optical Engineering, School of Physics Science and Engineering, Tongji University, Shanghai 200090, China

[43]School of Physics and Astronomy, Sun Yat-Sen University, Zhuhai 519082, China

[44]Mullard Space Science Laboratory, UCL, Holmbury St Mary, Dorking, Surrey, RH56NT, UK

[45]Sezione di Torino, Istituto Nazionale di Fisica Nucleare, Via Pietro Giuria, 1, Torino 10125, Italy

[46]State Key Laboratory of Transducer Technology, Shanghai Institute of Microsystem and Information Technology, Chinese Academy of Sciences,Shanghai, 200050, China

[47]Shanghai Industrial Technology Research Institute, Shanghai 201800, China

[48]European Space Agency, Keplerlaan 1, PO Box 299 NL-2200 AG Noordwijk, The Netherlands

[49]Space Research Centre, Department of Physics and Astronomy, University of Leicester, Leicester, LE17RH, UK

[50]INAF – Osservatorio Astronomico di Cagliari, Via della Scienza 5 - 09047 Selargius (CA), Italy

[51]Centro de Astrobiologia (CSIC-INTA), Dep. de Astrofsica, ESAC, Madrid 28850, Spain

[52]Frentech Aerospace s.r.o. Jarní 48 CZ S 614 00 Brno

[53]Electrical and Electronic Engineering, Istanbul Technical University, Ayazağa Campus, Turkey

[54]Tuorla Observatory, Department of Physics and Astronomy, University of Turku Väisäläntie 20, Piikkiö, FIN, 21500, Finland

[55]Nordita, KTH Royal Institute of Technology and Stockholm University, Stockholm, SE, 10691, Sweden

[56]State Key Laboratory of Transient Optics and Photonics, Xi'an Institute of Optics and Precision Mechanics, Chinese Academy of Sciences, Xi'an 710119, China

[57]TIFPA, Istituto Nazionale di Fisica Nucleare, Via Sommarive 14, 38123 Povo, Trento, Italy

[58]School of Microelectronics, Shanghai University, Shanghai, 200444, China

[59]TÜBITAK-UZAY Space Technologies Research Institute, Ankara, Turkey

[60]Institute of Physics, Silesian University in Opava, Bezrucovo nam. 13, CZ-746 01 Opava, Czech Republic

[61]Anton Pannekoek Institute for Astronomy, University of Amsterdam, Amsterdam 1098 XH, The Netherlands

[62]State Key Laboratory of Advanced Welding and Joining, Harbin Institute of Technology, Harbin 150006, China

[63]School of Chemistry and Chemical Engineering, Harbin Institute of Technology, Harbin 150001, China

[64]Nicolaus Copernicus Astronomical Center, Polish Academy of Sciences, Bartycka 18, PL-00-716 Warszawa, Poland

ABSTRACT

The enhanced X-ray Timing and Polarimetry mission (eXTP) is a flagship observatory for X-ray timing, spectroscopy and polarimetry developed by an International Consortium. Thanks to its very large collecting area, good spectral resolution and unprecedented polarimetry capabilities, eXTP will explore the properties of matter and the propagation of light in the most extreme conditions found in the Universe. eXTP will, in addition, be a powerful X-ray observatory. The mission will continuously monitor the X-ray sky, and will enable multi-wavelength and multi-messenger studies. The mission is currently in phase B, which will be completed in the middle of 2022.

Keywords: black hole, neutron star, X-ray timing, X-ray polarimetry, equation of state, extreme gravity, extreme magnetism, extreme density

---

Further author information: (Send correspondence to Shuang-Nan Zhang)
Shuang-Nan Zhang: E-mail: zhangsn@ihep.ac.cn

1. INTRODUCTION

The enhanced X-ray Timing Polarimetry mission (eXTP) is a large, flagship mission for Astronomy and Astrophysics that will lead the spectral-timing-polarimetry studies of the X-ray Universe in the late 20s and early 30s. The mission is being developed by a large International Consortium, which includes institutions from China and 11 European countries, and is led by the Institute of High Energy Physics (IHEP) of the Chinese Academy of Sciences (CAS). The three core objectives of eXTP aim at answering key open questions of fundamental physics: 1. The physical nature of cold ultra-dense matter; 2. the behaviour of matter and light in the space-time shaped by strong-field gravity; 3. the astrophysics and physics of the strongest magnetic fields in nature. The matter inside neutron stars (NSs), the space-time in the vicinity of the Black Hole (BH) horizon, and the extremely magnetized vacuum close to magnetars and accreting pulsars are uncharted territories of fundamental physics. NSs and BHs provide a unique arena for their exploration. The eXTP mission will revolutionize these fundamental areas of today's research by high precision X-ray observations of NSs across the magnetic field scale and BHs across the mass scale.

In addition to investigating questions of fundamental physics, eXTP will enable excellent observatory science opportunities, providing observations of unprecedented quality on a variety of galactic and extragalactic objects. eXTP's wide field monitoring capabilities will also be crucial in the context of multi-messenger astronomy by detecting and monitoring the electro-magnetic counterparts of gravitational waves and neutrino cosmic sources. eXTP will operate at the time of operation of major facilities in multi-messenger astronomy, such as the second generation of the GW interferometer network (e.g., aLIGO, aVIRGO, KAGRA, LIGO-India), the neutrino observatories IceCube-Gen2 and KM3NeT, and other multiwavelength facilities including SKA, LOFAR and FAST (radio), HERD (GeV to TeV), CTA and LHAASO (from TeV to PeV), and ALMA (mm). eXTP observations will be of crucial interest to a very wide international community, well beyond the X-ray astronomy community.

What makes eXTP unique in comparison to other existing X-ray missions, including those currently in development, is its unprecedented combination of broad-band large collecting area, polarimetric capability, and spectral resolution. Owing to this combination, eXTP is expected to open an entire new window in X-ray observations: simultaneous spectral-timing-polarimetry. eXTP will thus be complementary to ATHENA in terms of science and payload. The current baseline of the scientific payload includes four science instruments: the Spectroscopy Focusing Array (SFA), the Large Area Detector (LAD), the Polarimetry Focusing Array (PFA), and the Wide Field Monitor (WFM). The instrument configuration and key specifications are summarized in Table 1.

The mission is proposed to be launched in a low-earth orbit at an altitude of ≤570 km. The inclination of the orbit is ≤2.5 deg so that the instruments can operate in a low particle density environment to minimize radiation degradation and particle-induced background. The baseline launcher is the Chinese Long March-5 (CZ-5) vehicle. Nominal science operations will last for 5 years. eXTP observations will comprise standard (planned) pointing observations, as well as targets of opportunity (ToO) triggered by WFM or other astrophysical facilities. The WFM trigger time and position will be provided to the end user in less than 30 s after on-board detection of the event. The programme will devote a significant fraction of observations to the core objectives. A substantial fraction will also be devoted to observatory science, through a fully open Guest Observer programme, and to coordinated multi-messenger programmes. The WFM data will be released to the astronomy community immediately. Data of the SFA/LAD/PFA will be released when the data proprietary period expires. The Consortium aims at a proprietary period of one year. A fraction of the total observation time will be allocated as DDT, which will be primarily used to respond to unanticipated or *ad hoc* ToO, the data of which will be openly released immediately. The mission is currently in phase B in China, which will be completed by the end of 2022. The launch of eXTP is planned for 2027.

2. SCIENTIFIC GOALS OF THE MISSION

The three core objectives of the eXTP mission aim at answering key open questions of fundamental physics: 1. The physical nature of cold ultra-dense matter; 2. the behaviour of matter and light in the space-time shaped by strong-field gravity; 3. the astrophysics and physics of the strongest magnetic fields in nature. The general introduction on the eXTP mission, including its the core objectives and observatory science, has been given in

Table 1. The instrument configuration and key specifications.

Instrument	SFA	LAD	PFA	WFM
Configuration	9 telescopes	40 modules	4 telescopes	6 cameras
Optics or collimator	Wolter-I, Nickel F = 5.25 m	capillary-plate collimators	Wolter-I, Nickel F = 5.25 m	coded mask
Detector	19-pixel Silicon Drift Det. (SDD)	SDD	Gas Pixel Detector (GPD)	SDD
Energy range	SFA	LAD	PFA	WFM
Effective area or FoV	$\geq$0.6 m^2 @ 1-2 keV 0.4 m^2 @ 6 keV	3.0 m^2 at 8 keV	500 cm^2 @ 2 keV 300 cm^2 @ 3 keV	FoV $\geq$ 3.1 sr
Energy res. (FWHM)	180 eV @ 6 keV	260 eV @ 6 keV	25% @ 6 keV	$\leq$500 eV @ 6 keV
Time res.	10 µs	10 µs	10 µs	10 µs
Remarks	unprecedented effective area in the soft X-ray energy range	high throughput; effective area is a factor of 5-10 larger than any previous mission	$\sim$5 times the area of IXPE, X-ray polar. Pathfinder by NASA; Min. Detectable Polarization $\sim$3% in 2-8 keV energy range	peak sensitivity: 1 Crab in 1 s and 5 mCrab in 50 ks (5σ source); Point source localization $\leq$1'

the white paper on 'The enhanced X-ray Timing and Polarimetry mission—eXTP' by Zhang et al. (2019).[1] Here we provide an update on the scientific goals of the eXTP mission.

2.1 The Physical Nature of Ultra-Dense Matter

Understanding the properties of ultra-dense matter and determining its equation of state (EOS) is one of the most challenging problems in contemporary physics. The science rationale at the core of this scientific objective is discussed in detail in the white paper on 'Dense Matter with eXTP' by Watts et al. (2019).[2] Neutron stars (NSs) represent a unique regime of high baryonic density (up to ten times the density of normal atomic nuclei) and low temperature (T $\ll$ 1 MeV from a few minutes after formation). This is well illustrated in Figure 1.

In addition to matter that has high neutron-proton asymmetry, exotic states of matter such as hyperons or deconfined quarks, color superconducting phases may also appear. It is this uncharted territory of strong interaction that eXTP aims at exploring. Connecting NS parameters to strong interaction physics can be done because the forces between the nuclear particles set the stiffness of NS matter.[3] This is encoded in the (EOS), the thermodynamical relation between pressure, energy density and temperature.[4,5]

There is a one to one map from the EOS to the Mass-Radius (M-R) relation, forming a unique bidirectional mapping between EOS and M-R relation. Some examples are shown in Figure 2. The mass and radius of NS determine the space-time in the NS vicinity and therefore can be measured through astrophysical observations. We can then in reverse infer the properties of the EOS and the microphysics which determines these properties. In other words, the validation of model calculations by the Quantum Chromo Dynamics (QCD) is translated into a precise observation of the masses and radii of NSs. To reach this goal a precision of simultaneous measurements of the NS mass and radius is required to be within 3 and 4%.

The first eXTP top science goal is as it follows: The equation of state of cold ultra-dense matter will be determined by measuring both mass and radius for several neutron stars, using different techniques that can be compared and cross-validated.

eXTP will use several techniques to study the EOS of matter in NS.[2,5] eXTP will measure the masses and radii of accreting, nuclear-powered and rotation-powered millisecond X-ray pulsars by modelling their pulse profiles. The stars' fast spin and strong gravity affect the radiation from surface hot spots, which produce pulsations affected by relativistic beaming, time dilation, red/blue-shifts, gravitational light bending and frame dragging.
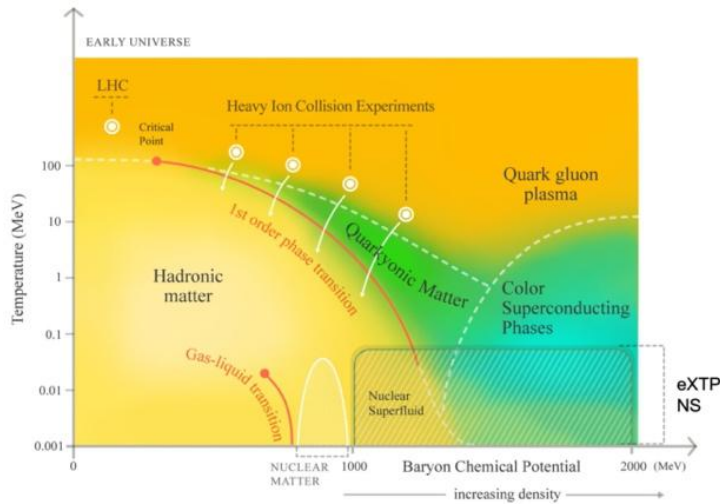
Figure 1. States of baryonic matter in the parameter space of temperature against baryon chemical potential. Note that 1-2 GeV corresponds to ~1-6 times the density of normal atomic nuclei. Neutron stars access unique states of matter that cannot be created: nuclear superfluids, strange matter states with hyperons, deconfined quarks, and color superconducting phases.
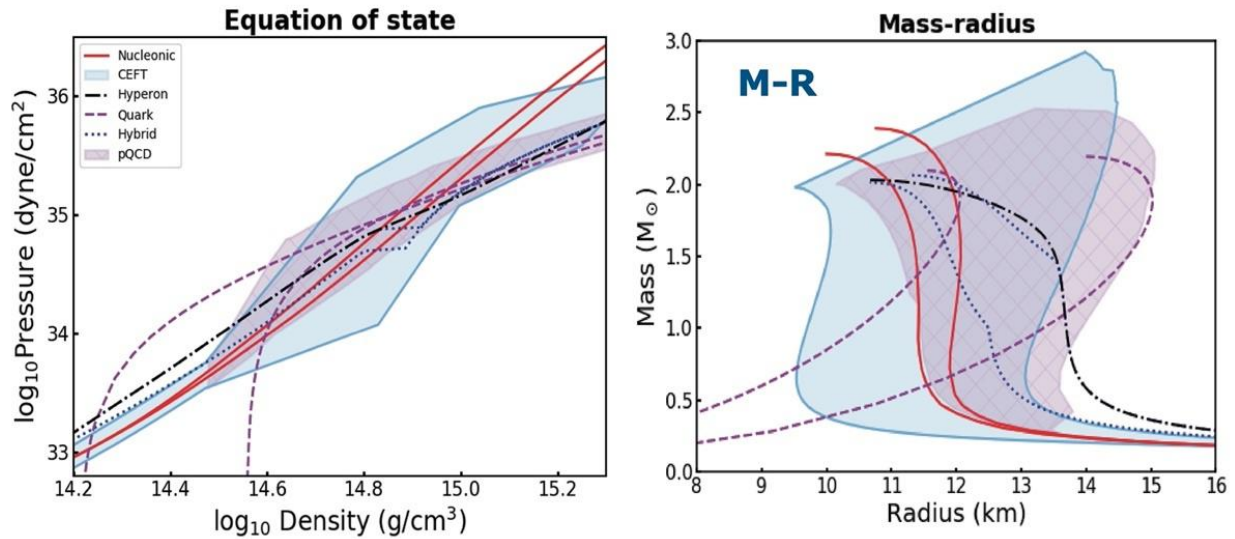
Figure 2. In the left panel the pressure density relation and on the right panel the corresponding mass radius relation for some example models with different microphysics. Nucleonic models are taken by Ref. 6. Quark models from Refs. 7,8. Hybrid and Hyperon models from Ref. 9 and Ref. 10. Range of nucleonic EOS based on Chiral Effective Field Theory (CEFT) are from Ref. 11. pQCD: range of nucleonic EOS from Ref. 12 that interpolate from CEFT at low densities and match to perturbative QCD (pQCD) calculations at higher densities than shown in this figure. Each of the curve in the left panel biunivocally corresponds to a curve in the right panel.
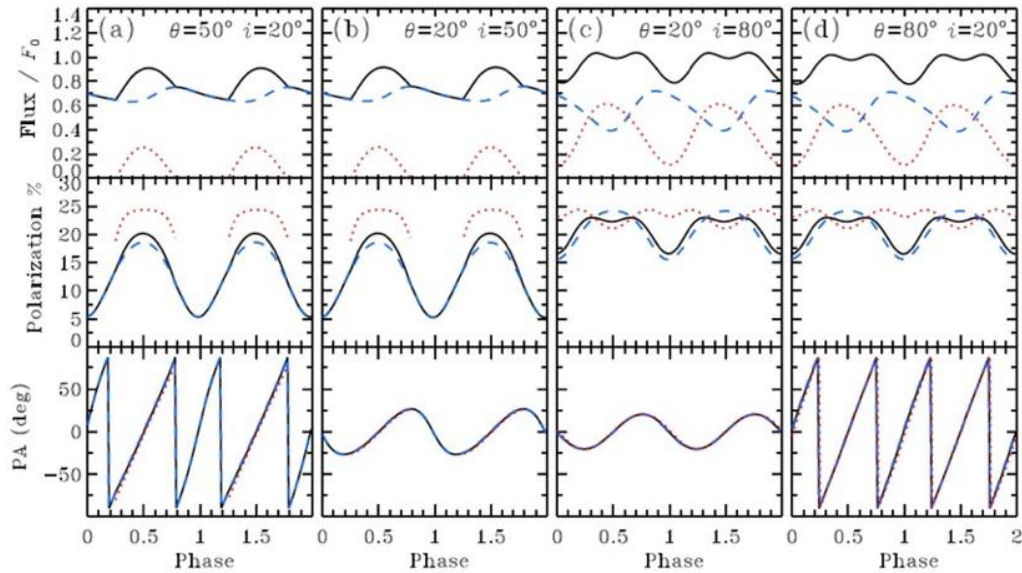
Figure 3. The pulse profiles as well as the phase dependence of the polarization degree (PD) and Polarization angle (PA) are shown. The black solid shows the contribution of two antipodal spots. Here i is the observer inclination and θ is the hotspot colatitude. The pulse profiles and PD are degenerate with respect to i and θ, while PA shows a dramatically different behavior so that both angles can be obtained.[17]

Information about mass M and Radius R is encoded in the pulse profile. Since we can measure energy dependent pulse profiles, we can recover M and R. A wide literature of the last few decades has established how to model the relevant aspects (Ref. 13 and references therein). The technique has been already tested sufficiently for a few rotation-powered pulsars with NICER (see e.g., Ref. 14,15) to provide a proof of concept. NICER has measured M and R at 10% uncertainties in two systems, and highlighted key issues in the calibration and analysis. The sample pulsars studied with eXTP will be much large, up to 20 objects and will include rotation- accretion- and nuclear- powered pulsars. Observing a large sample of neutron stars will allow us to study the EOS across a wider range of central densities, mapping the EOS more fully and probing any potential phase transitions with finer resolution. In the case of eXTP results can be cross-validated: several sources have both accretion-powered and thermonuclear hotspots, for example, allowing independent cross-tests for the same source. Other complementary constraints include phase-average burst spectral modelling for photospheric radius expansion (PRE) bursts. In addition, the polarimetry capabilities of eXTP will provide an essential knowledge of the geometrical factors of the pulsars, further improving the statistical constraining power via degeneracy breaking.[16] Radiation emitted by hotspots is expected to be linearly polarised because the opacity is dominated by electron scattering.[17]

The observed polarization degree (PD) and polarization angle (PA) change with the rotational phase φ following variations of the angle between the spot normal and the line-of-sight, and of the position angle of the projection of the hotspot normal on the sky. The pulse profile, and the phase-dependence of the PD and PA are shown in Figure 3. In conclusion, to measure M and R of NSs, eXTP will use different techniques: A summary of the techniques is shown in Figure 4.

eXTP can also provide an independent constraint on EOS by filling out the accreting NS spin distribution, searching for pulsations in 35 accreting NSs covering a range of luminosities and inclinations, reaching rms amplitude detectability limits (for short duration $\sim$100 s) with intermittent accretion-powered pulsations of 0.05% for bright sources and 2% for faint sources; for weak persistent accretion-powered pulsations, 0.01% (bright) and 0.5% (faint); for oscillations during Type I bursts, 0.5% in the burst tail and 1.5% in the burst rise. Figure 5 shows an example of the expected eXTP measurement.

Gravitational wave (GW) observations of compact binary inspirals allow independent constraints on the EOS by measuring mass and tidal deformability. Constraints can also be derived from electromagnetic counterparts

Figure 4. Different techniques can be used to measure the M and R of different classes of NSs. In some cases, several techniques can be applied on the same object, providing powerful cross validation of the results.
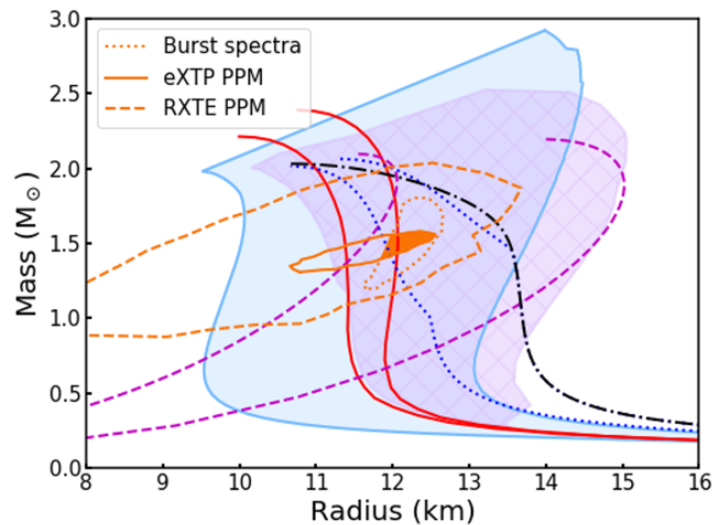
Figure 5. Constraints from pulse profile modelling and burst spectral fitting expected for eXTP. The orange dashed contour shows 1 σ constraints obtained with RXTE measurements of the accreting millisecond pulsar SAX J1808.4-3658. The constraints expected from pulse profile modelling (PPM) with spectral timing observations with SFA and LAD observations, and polarimetric information with PFA are shown as the solid orange contour. Spectral evolution during PRE bursts (shown by this pulsar) produces more perpendicular contours on M and R.[18] All combined methods provide the orange area that indicate constraints on M and R of a few percent. The source also shows burst oscillations, that could provide entirely independent constraints.
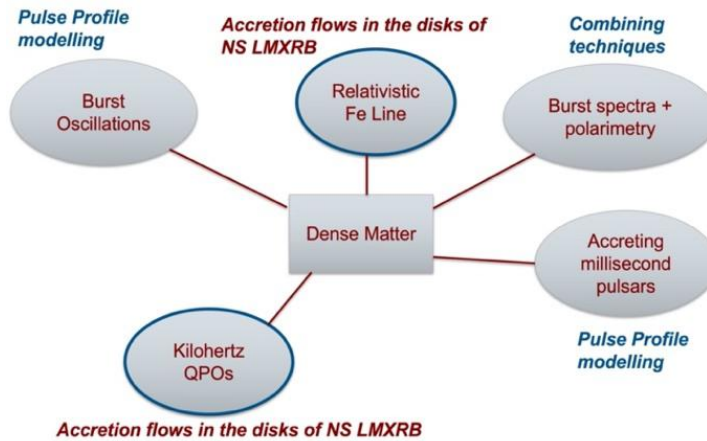
Figure 6. Different techniques can be used to measure the mass and spin of different types of BHs. In some cases, techniques can be applied on the same object, providing powerful cross validation of the results. A description of these techniques can be found in Ref. 23.
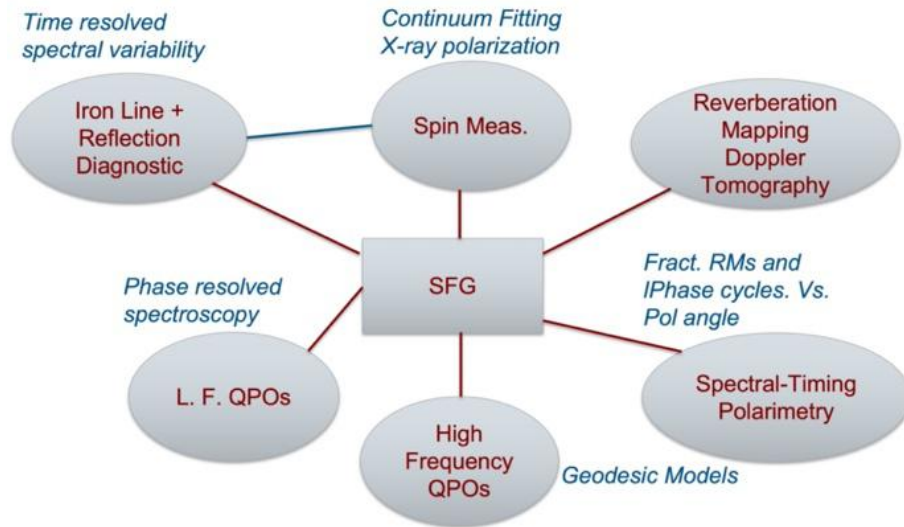
and (potentially) post-merger ringdown signals. There is a lot of power in combining constraints from PPM and GW, as is already being done for NICER/LIGO/VIRGO (see e.g. Ref. 19). However, comparison of independently-derived constraints is also essential, to check for potential modelling systematics that might affect either or both techniques. This is important given potential tension with EOS constraints derived from nuclear physics experiments (PREX-II, Ref. 20).

2.2 Strong Field Gravity

The motion of accreting plasma near super-massive black holes (SMBHs) hosted in Active Galactic Nuclei (AGN) and stellar-mass black holes (BHs) in X-ray binaries (XRBs) provides a powerful diagnostic to study the very deep potential well generated by the central object. Strong-field gravity can be parametrized by BH mass and spin, which are encoded in X-ray emission from the inner accretion flow. This emission depends on the metrics and therefore on the spin, since the Kerr metric predicts that the location of the inner edge of a BH accretion disk depends monotonically on the spin.[18] Astrophysical BHs which cover 8-9 orders of magnitude in mass, allowing a unique test of the scale invariance of gravitational effects and a link between the behaviour of accretion flows in stellar mass systems versus those around SMBHs.[21] In addition, understanding the spin distribution of stellar-mass BHs provides key information on the BH formation process,[22] while measurement of spins in AGN will probe cosmic BH spin evolution.

The second top science goal of eXTP is summarized as follows: To unveil how matter behaves in the strong gravity regime, the structure and dynamics of the innermost accreting regions around BHs will be mapped and BH mass and spin measured, across all BH mass scales. To this end, eXTP will exploit a variety of independent and intersecting techniques: reflection and thermal continuum spectroscopy, precision measurement of high-frequency QPOs, spectral-timing-polarimetry of quasi-periodic oscillations and Fe emission line reverberation and tomography.

The science rationale at the core of this scientific objective is discussed in detail in the eXTP white paper on 'Accretion in Strong Field Gravity with eXTP' by De Rosa et al. (2019).[23] A summary of the techniques is shown in Figure 6. The eXTP observations will allow us to disentangle complex spectra, such as additional absorption and broad reflection continuum features in AGN and the combination of disk blackbody, coronal continuum and reflection in XRBs, thus enabling much more accurate measurements of relativistic reflection features in AGN and XRBs and the disk thermal emission in XRBs. An example is shown in Figure 7.
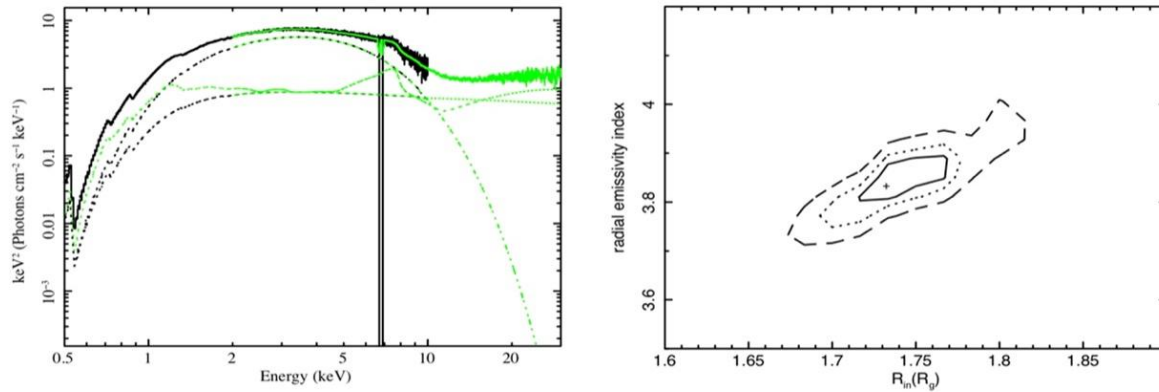
Figure 7. In the left panel we show the eXTP simulated SFA + LAD spectrum obtained in only 100 s integration of a 0.5 Crab, spin $a^* = 0.97$ XRB BH. Simulation of the soft state spectrum included a thermal disk component, hard Comptonized continuum, relativistic reflection features, and highly photoionized absorption due to outflows (an example is GRO J1655-40). In the right panel, the confidence levels at 1, 2, 3σ for the radial emissivity index and the inner radius of the disk in units of the gravitational radius $R_g = GM/c^2$ are shown. Precision is 2% and 5% respectively. The unprecedentedly short timescale will allow us to observe the variability of the structure of the innermost region on a timescale comparable to that of the fastest changing components like winds and jets.
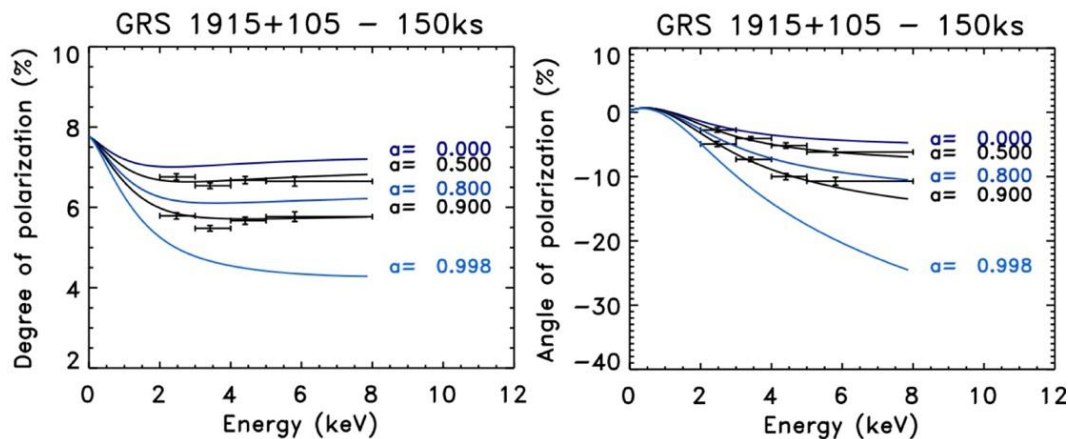

Figure 8. Simulated eXTP PFA measurements of polarization degree (left panel) and polarization angle (right panel) as a function of energy expected from a 150 ks exposure of GRS 1915+105 in the soft state. Blue and black curves show the expected dependencies of the polarization quantities on spin, while the black points show the simulated data using the synthetic curves. It can be seen that the spin can be estimated with a very high precision (around 5%)

As we show in Ref. 23, the BH spin can be obtained independently of spectral fitting of relativistically broadened lines or thermal continuum, by measuring the rotation with energy of the polarization angle of the disk emission. In GR, the rotation angle of the polarization plane of the disk radiation depends on the emitting point and it is larger the closer to the BH the emitting point is. Since the harder photons come from the inner regions, they suffer a larger rotation. In Figure 8 we show an example based on a 150 ks exposure of GRS 1915+105. High Frequency Quasi-Periodic Oscillations (HFQPOs), at frequencies of 40-450 Hz can probe timescales close to or at the Innermost Stable Circular Orbit (ISCO). Their origin is not well known, but they could occur due to a precessing inner flow or orbiting inhomogeneities in the disk. Models can convert pairs of HFQPOs into BH masses and spins. The identification of higher modes can break the model dependent degeneracies (see e.g., Ref. 24). However, what is needed is a leap forward in HFQPOs detection, that might go well beyond the tip of the iceberg of the current detections, towards weaker signals expected in many GR models. As shown in Figure 9, eXTP has tremendous potential.

In other words, the high-count rates obtained by the SFA and LAD allow detection and tracking of BH
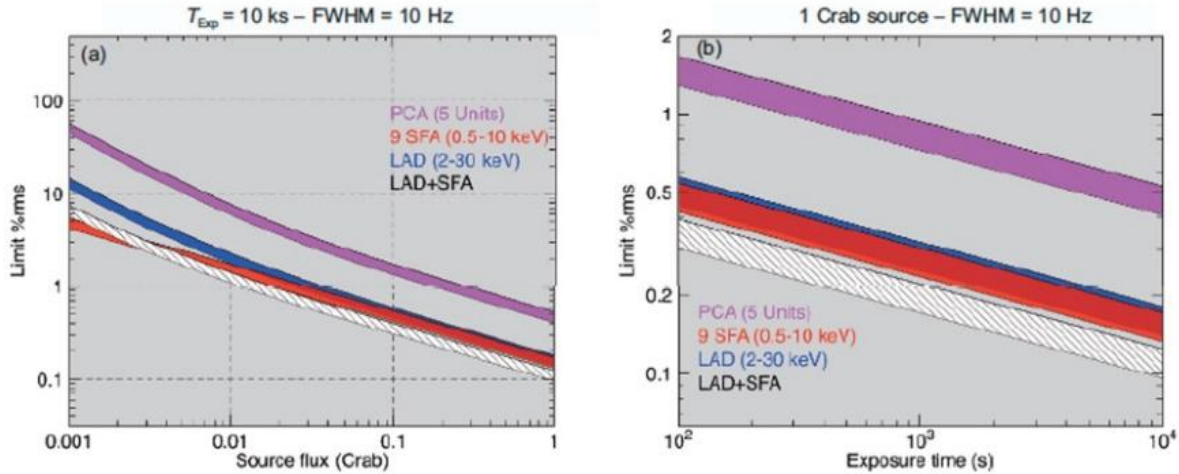
Figure 9. (a) Simulated eXTP sensitivity (for detection against the Poisson noise level) in fractional rms for a QPO of arbitrary frequency (FWHM=10 Hz) as a function of flux (10 ks exposure). Panel (b): same as for a source of 1 Crab but as a function of exposure. Each stripe marks the 3 and 5σ significance levels. Different colors for different instruments. The sum of LAD and SFA is in white. The LAD only in blue. The SFA alone in red.

HFQPOs in XRB down to low rms amplitudes, allowing us to determine their origin and use them as an independent diagnostic of BH spin and a potential test of the dynamics of matter close to the BH.

With the combined spectral-timing-polarimetry techniques eXTP will cleanly separate the spectral components from the innermost strong gravity region, variable on short timescales, from those at larger scales which will vary much more slowly. In the hard intermediate state of BH, there exists also a low-frequency QPO signal likely caused by the Lense-Thirring precession. The precession originates from the misalignment between the BH spin and the angular momentum of the disk. eXTP can perform tomography and timing-polarimetry study to constrain this misalignment angle. eXTP in fact will also measure changes in polarization degree and angle with QPO phase, giving an additional powerful and independent probe of the variations in coronal geometry associated with the QPO modulation.

In AGN the BH masses can be inferred from variability in the Fe K-line (disk tomography). Reverberation (radiation echoing) of the variability of an incident hard continuum from the corona off the disk leads to light travel time lags between the different components. These lags constrain the geometry on an absolute length scale (km), allowing us to constrain BH masses, as well as changes in the inner geometry associated with different accretion states (Figure 10).

The BH spin and mass estimates obtained by eXTP for XRBs probe a different population of BH than those studied with GW emission, which form from massive stellar binaries, so eXTP measurements will be highly complementary with the GW measurements. BHs in high mass XRB already appear to have systematically higher spin than those observed via GW, which are consistent with zero spin, suggesting a different formation channel of BH in high mass XRBs vs those in massive binaries (e.g. Ref. 21). Thanks to the cross-comparison of multiple techniques to estimate mass and spin, the eXTP measurements will be of comparable or better precision and accuracy than those obtained for GW events, allowing a clear comparison of the three different BH populations, i.e. those formed in: massive binaries, high mass XRBs and low mass XRBs.

2.3 Strong Magnetism

NSs can host the strongest magnetic fields observed in Nature, up to B$\sim10^{14-15}$ G. They are therefore natural laboratories to study the physics and astrophysics of strong magnetic fields.

The third top science goal of eXTP is summarized as it follows: The physics of the strongest magnetic fields in nature will be constrained by studies of the spectral, timing and polarization properties of magnetars and
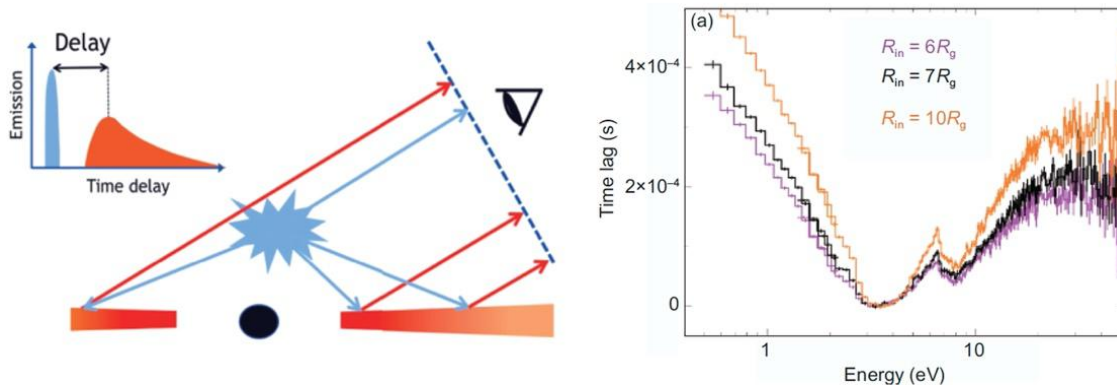
Figure 10. (Left panel) Conceptual schematic of X-ray reverberation. The coronal emission (from the blue spot) is reflected by the disk resulting in a light-travel time delay of the reflected emission which constrains the light-travel time. In strong gravitational fields strongly curved light-travel paths are expected that can be constrained with reverberation measurements. (Right panel) Simulated eXTP (100 ks) exposure lag vs. energy spectrum of a 10 solar masses BH, for 1 Crab hard state. Different inner radii can be easily distinguished. Thanks to the broad band of eXTP (SFA and LAD), the hard lags can be obtained for the blackbody component, the Fe K line and the reflection hump. This allows multiple independent measurements of the geometry and relativistic effects of the innermost part of the accretion flow.
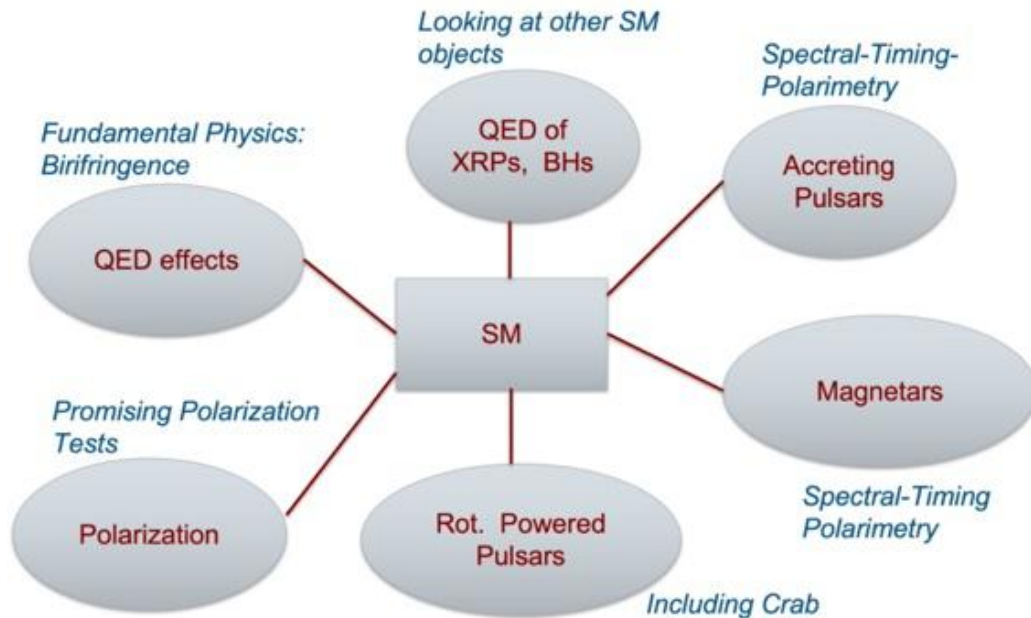
Figure 11. Different techniques can be used to probe the physics and astrophysics of strong magnetism, mainly in extremely magnetized (magnetars) and highly magnetized (accreting pulsars) NSs. QED effects could be also tested in BHs. These techniques will use spectral timing and polarimetry information.[25]

accreting X-ray pulsars. Fundamental physics effects predicted by Quantum Electro Dynamics (QED) will be tested. Different complementary approaches will be used to reach this objective (Figure 11).

The science rationale at the core of this scientific objective is discussed in detail in the eXTP white paper on 'Physics and astrophysics of strong magnetic field systems with eXTP' by Santangelo et al. (2019).[25] eXTP will unveil the physics and astrophysics of magnetars, NSs with B$\sim10^{14-15}$ G, whose decay or reconnections powers their high energy emission in X-rays and even gamma rays. Magnetars are thought to manifest as anomalous X-ray pulsars (AXPs) and soft gamma repeaters (SGRs), with spin periods of $\sim$(1-10)s and period derivatives of $\sim(10^{-15}$-$10^{-10})$s/s. Magnetars are characterized by their bursting activity at unexpected times, and eXTP

Figure 12. Phase averaged Polarization Fraction for the thermal radiation emitted from a transient magnetar at the peak of the outburst computed for different values of the viewing angles χ and ϵ respectively the angle between the line of sight and the spin axis, and the magnetic and spin axis.
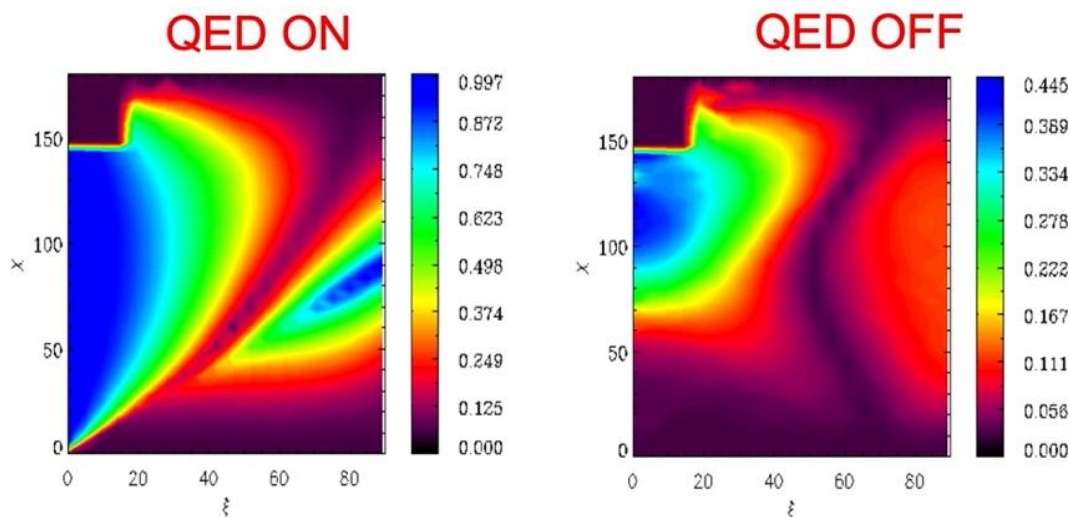
will have an unprecedented capability to study their bursts, outbursts, and timing behaviours. eXTP will allow to perform systematic asteroseismology using magnetar short bursts and intermediate flares, to study the polarization and spectral properties of these events, to detect magnetar glitches with unprecedented sensitivity and to prove magnetar free precession: this is essential to unveil the nature of magnetars and to answer fundamental questions in magnetospheric physics and basic, fundamental physics. Phase and/or energy dependent absorption spectral features can be systematically observed by eXTP in AXPs/SGRs and X-ray dim isolated NSs (XDINSs), enabling the cross-comparison (in both, intensity, and topology) of the magnetic field configuration in the vicinity of the NS in different classes of sources. eXTP will constrain the geometry of the surface magnetic field of magnetars and XDINSs by detecting energy and phase-dependent proton cyclotron lines, resulting from resonant scattering in the presence of magnetic structures close to its surface.

In addition, eXTP will clarify the geometry of the emission region and the origin of the observed phase-dependence of X-ray spectra in accreting pulsars using pulse phase and luminosity resolved spectral and polarimetry measurements. This will shed light on basic properties of the NS such as compactness, magnetic field strength and configuration. These studies will be complemented by investigating - for the first time with eXTP - variability on timescales comparable and below the pulse period (down to microseconds!). Pulse to pulse spectroscopy will allow to probe luminosity dependence of the emission region properties even in persistent pulsars where the average flux remains constant, whereas short variability will allow to probe structure of the accretion flow and stability of the emission region itself ("photon bubble" oscillations). QED effects, like vacuum birefringence, can also be tested by phase-averaged and pulse phase-resolved polarimetric measurements of magnetars, and pulse phase resolved polarimetry measurements of accreting pulsars (see Figure 12). For X-ray pulsars, QED is considered an essential element in the modelling of the emission region, which, given the luminosity dependence of the emission region geometry, will allow to independently test the underlying assumptions regarding the magnetic field strength and configuration.

2.4 Observatory and Multi-messenger Astrophysics

Observatory science. In addition to the core science goals envisioned for eXTP, the mission will be a powerful X-ray observatory since it has unique capabilities to contribute to a wide variety of other scientific fields. The potentials of eXTP as an observatory are presented in detail the white paper on 'Observatory science with eXTP' by in 't Zand et al. (2019).[26] The science fields investigated consist of goals related to accretion physics, stellar evolution, cosmology and galaxy evolution, and nuclear and particle physics. Objects or events like thermonuclear bursts, fast radio bursts, high and low mass X-ray binaries, radio quiet and radio Loud AGN,

Figure 13. eXTP will operate in the epoch of truly multi-wavelength and multi-messenger astrophysics. 2G refers to second generation GW interferometers: aLIGO. Advanced Virgo, KAGRA and LIGO India. 3G refers to the third generation that will start in the mid thirties: Einstein Telescope and Cosmic Explorer. IceCube (and its extension Gen-2) and KM3NeT will significantly open neutrino astronomy. CTA is expected to be deployed soon and will boost our knowledge of the TeV Universe. LOFAR, SKA and ALMA are large enterprises in the radio and mm band. The large radio telescope FAST and ultra-high energy gamma-ray observatory LHAASO in China are operational, but not shown.

tidal disruption events, gamma ray bursts, ultra-luminous X-ray sources, supernovae, and stars will be subjects of intense research with eXTP. eXTP will also search for exotic particles, like axions, sterile neutrinos and dark photons. A significant fraction of the observing time (∼50%) will be allocated to observatory science based on peer reviewed proposals.

Multimessenger astrophysics. The WFM, with its unprecedented combination of field of view and imaging down to 2 keV, makes eXTP a discovery machine of the variable and X-ray transient sky. The WFM will reveal many new sources for follow-up with the SFA, PFA, LAD and other facilities. The WFM will be monitoring daily hundreds of sources, to catch unexpected events and provide long-term records of their variability and spectroscopic evolution. eXTP will be a unique, powerful X-ray partner for other new large-scale facilities available in the 2020s: GWs and neutrino experiments, FAST, SKA and LOFAR in the radio, LSST and E-ELT in the optical, the High Energy cosmic-Ray Detection (HERD, to be onboard China's Space Station from 2027) at GeV to TeV, and CTA and LHAASO at TeV energies. This is shown in Figure 13.

The detection of GW170817, results of the coalescence of two NS[27] and of the associated GRB170817,[28] impressively opened the era of multi-messenger astronomy. By the same epoch the first identification of a cosmic neutrino source with the flaring Blazar TXS0506+056 at redshift z=0.34[29] similarly impacted astrophysics. eXTP will provide a vital electromagnetic (EM) complement to all classes of GWs studies. In the high-frequency (LIGO/VIRGO) bands, the WFM on eXTP would instantly provide positions accurate enough for follow-ups with integral field units (IFUs), or for single field imaging. This enables nearly-immediate spectroscopic observations, that will open up new parameter space both through brighter, higher S/N spectra, and earlier phenomenology. As
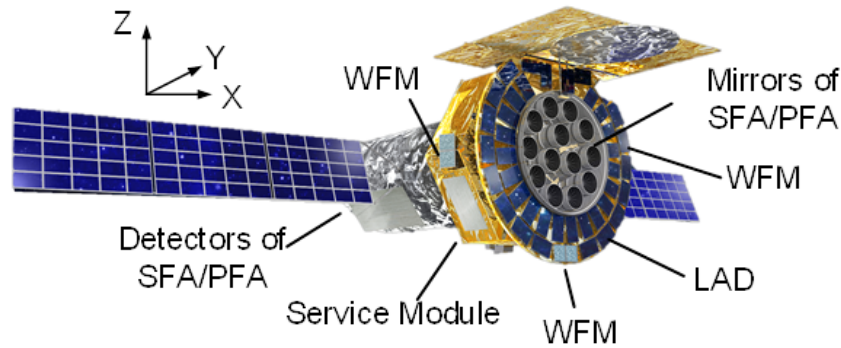
Figure 14. Artistic view of the eXTP satellite. The science payload consists of four instruments: the focused SFA and PFA telescopes arrays, the large area instrument LAD, and the WFM to monitor a large fraction of the sky.

extensively discussed in[29] the prompt and precise localization of X-ray transient counterparts to compact binary mergers will be crucial, in the epoch of 2G GW detector network, that will include in the mid 2020s aLIGO, Advanced Virgo, KAGRA and LIGO-India. Key questions on the astrophysics of GRBs, like jet formation, launching and structure; on the role of NS-NS and NS-BHs mergers in the chemical enrichment of the Universe; on the expansion rate of the Universe during its evolution; on shock breakouts in core-collapse SNe could be answered by joint GW and EM observations.[29] Observations of cosmic neutrino sources in the EM band, that will become routinary with KM3NET and IceCube-gen2, will provide information on the acceleration mechanisms in celestial accelerators like Blazars or GRBs.

3. PROPOSED PAYLOAD

The current baseline of the scientific payload includes four science instruments: the Spectroscopy Focusing Array (SFA), the Large Area Detector (LAD), the Polarimetry Focusing Array (PFA), and the Wide Field Monitor (WFM). An artistic view of the eXTP satellite and the product tree of the proposed payload are shown in Figure 14 and Figure 15 respectively.

3.1 Spectroscopy Focusing Array (SFA)

The SFA consists of an array of 9 identical Wolter-I grazing-incidence X-ray telescopes (see Figure 16), and is mainly used for spectral and timing observations in the energy range 0.5-10 keV. Each telescope consists of one mirror assembly and one Silicon Drift Detector (SDD) camera at its focal plane. The angular resolution of the Wolter-I mirror is required to be less than 1 arcmin (HPD), which can reduce the background well when coupled with the electron diverter. Each telescope includes a 19-cell SDD array, whose energy resolution is better than 180 eV at 6 keV. The time resolution is 10 µs, and the dead time is expected to be less than 5% at 1 Crab. The total effective area of SFA is required to be larger than 6000 cm^2 at 1-2 keV, and the expected performance in comparison with other X-ray focusing telescopes can be seen in Figure 17.

The mirror assembly (including the electronic deflector) of each telescope is installed on the optical bench of the satellite. The focal plane camera is installed in the payload compartment, located on the other end of the satellite. The two compartments are connected by the telescope tube. The telescope tube is also the main support structure of the platform. In addition to ensuring the alignment accuracy of the two compartments, the telescope tube is also used to avoid stray light and prevent possible contamination.

The optics adopt the Wolter-I type structures to achieve a good imaging capability. Each mirror shell consists of a coaxial and confocal paraboloid and hyperboloid. A nested multi-layer structure is adopted to increase the effective area (45 shells in one mirror assembly). In consideration of the performance, weight, space environment and cost, the electroforming replication process is adopted to manufacture the mirror shells. Since the requirements of the optics in SFA and PFA are nearly the same, the same optical design and interfaces are adopted to simply the engineering implementation and reduce the risk. The main difference is the reflective
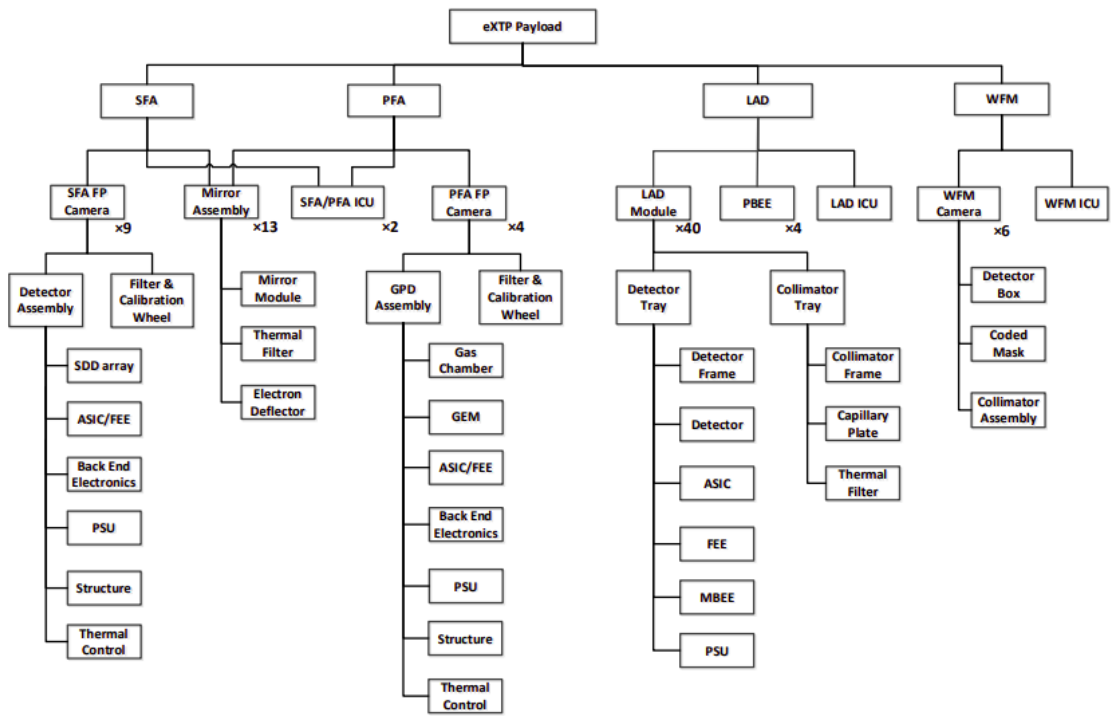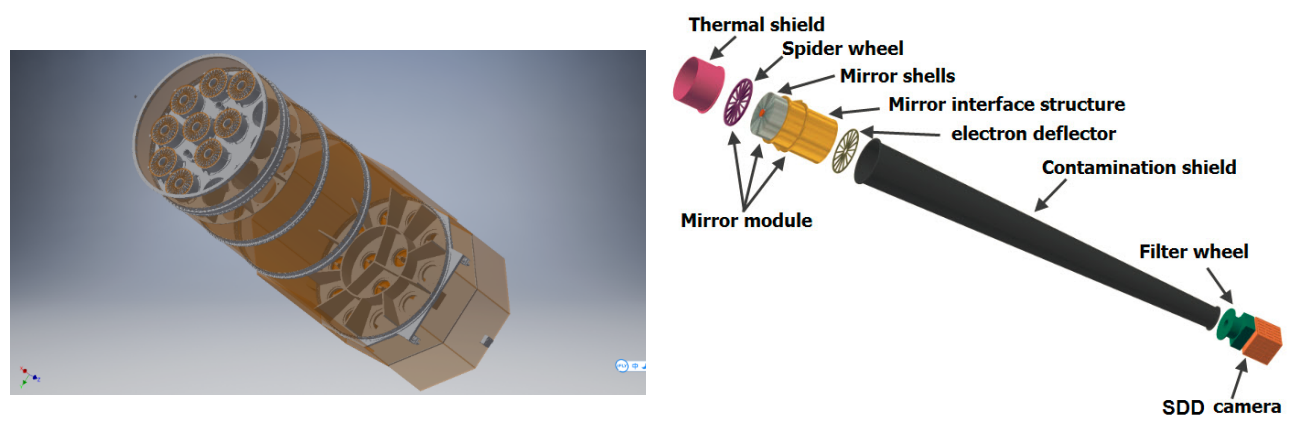
Figure 15. eXTP payload product tree.

Figure 16. Left panel: Layout of the nine SFA telescopes (the four empty holes are reserved for PFA telescopes); Right panel: Schematic structure of one SFA telescope.
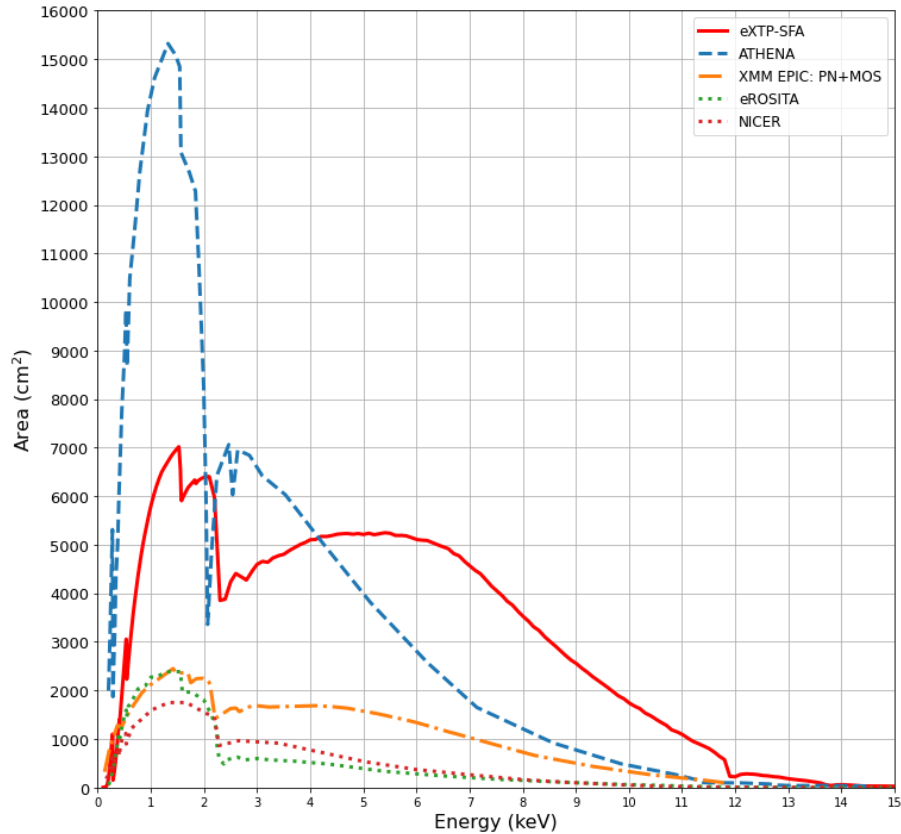
Figure 17. Comparison of the total effective area between SFA and other X-ray focusing telescopes.

Table 2. Main specifications of SFA/PFA mirror module

Parameters	Specification for one mirror module
Focal length	5250 mm
On-axis collecting area	$\geq$820 cm^2 at 1.5 keV (SFA) $\geq$800 cm^2 at 3 keV(PFA) $\geq$550 cm^2 at 6 keV
Angular resolution (HPD)	$\leq$1'(SFA) $\leq$30" (PFA, goal 15")
Energy range	0.3-10.0 keV
Refection surface	Surface material: gold (SFA), nickel (PFA) Micro roughness $\leq$0.5 nm (rms)
Envelope dimension	Diameter $\leq$ 600 nm
Working temperature	20$\pm$2°C
Weight	$\sim$125 kg

coating. The baseline design of SFA uses gold coating electroformed nickel shells, while PFA uses electroformed nickel shells directly. The main technical specifications can be seen in Table 2.

A mirror assembly includes electroformed nickel shells, spider, barrel, thermal shields, electron deflector, etc. (see Figure 18). 45 layers of coaxial and confocal mirror shells with different radii are fixed on the 24 spokes of the spider (equal-spaced radially) using epoxy glue. A thermal shield is installed on the aperture of the spider to block visible lights and infrared radiation and ensure the temperature stability of the mirror shells. Heater are glued on the side of the spokes and the support structure to actively control the temperature of the mirror
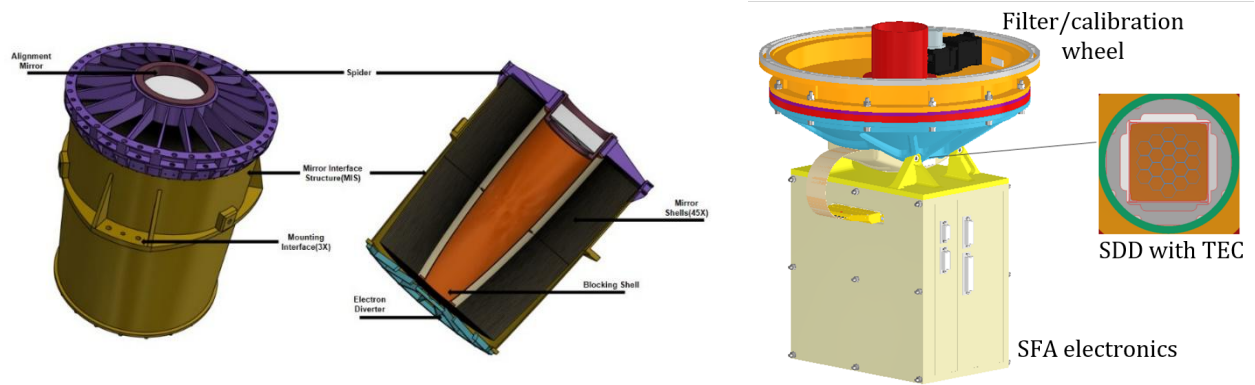
Figure 18. Left panel: One mirror assembly; Right panel: One SFA focal plane camera.

assembly. The electron deflector is installed at the exit of the mirror assembly, whose geometry is consistent with the spokes of the spider.

Each SFA focal plane camera consists of 4 parts (see Figure 18): an SDD array with 19 cells, an electronics box, a wheel mechanism, and a thermal electric cooler (TEC). The detection area of each SDD array is 5 cm^2, and each cell is hexagonal with an area of 26.6 mm^2 and an effective thickness of 450 μm. The detector box is mainly responsible for the signal amplification, shaping, AD conversion, and data acquisition of the SDDs.

The wheel mechanism is mainly composed of a mounting support, a driving component, a gear transmission component, a rotary transformer, and a rectangular sealing ring. It has 6 positions, which are optical blocking filters with 3 different thicknesses, in-flight calibration source (^{55}Fe), a thin polyimide protection layer for weak source observations, and a metal shutter for internal background measurement and protection from damage during launch and extreme solar events.

3.2 Large Area Detector (LAD)

The LAD is designed to perform, on a large collecting area, photon-by-photon observations of X-ray sources in the energy range of 2-30 keV (up to 80 keV in the expanded mode, for out-of-field-of-view burst events). SDD is used to measure the energy and time of arrival of the incident photons with time resolution better than 10 μs. The field of view of LAD is limited to ∼1° by the collimator, in order to reduce the backgrounds caused by the diffused sources and X-ray backgrounds. The LAD large area is achieved by a modular and intrinsically highly redundant design, which consists of 40 identical detection modules (called LAD module). Each module consists of a set of 4 × 4 large area SDDs and 4 × 4 capillary plate collimators, supported by two grid-like frames. The effective area of LAD is required to be larger than 3.0 m^2 at 8 keV, and the expected performance in comparison with other collimated X-ray telescopes can be seen in Figure 19. The details of the LAD design can refer to Ref. 30, 31 and the references therein.

3.3 Polarimetry Focusing Array (PFA)

The PFA consists of 4 identical telescopes optimized for X-ray imaging polarimetry, sensitive in the energy range of 2-8 keV. It offers energy, time, and spatially resolved X-ray polarimetry at high sensitivity, and is the only instrument on eXTP capable of imaging with a resolution of ≤30 arcseconds. The PFA features a sensitivity in polarimetry down to 3% given a 1 ks observation of the Crab. The total effective area of PFA is required to be larger than 300 cm^2 at 3 keV. The expected performance in comparison with IXPE can be seen in Figure 20.

The 4 PFA telescopes share the same optical design with SFA (Section 3.1, the angular resolution required for PFA is much better). The configuration of the PFA mirror module is also the same as SFA, except the reflection surface is nickel instead of gold.

The focal plane camera comprises detector and electronics boxes (see Figure 21). A detector box contains a Gas Pixel Detector (GPD) and filter wheel mechanism. There are two polarized calibration sources, three
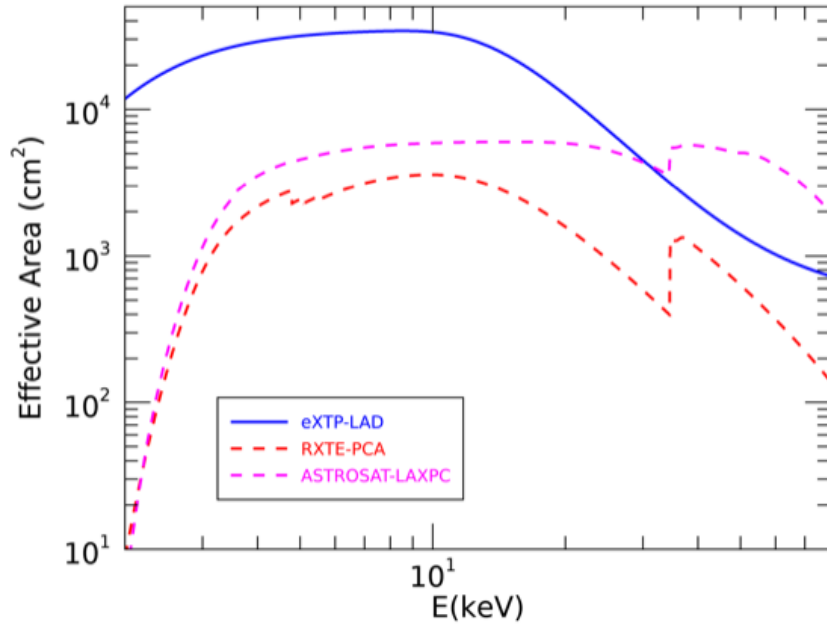
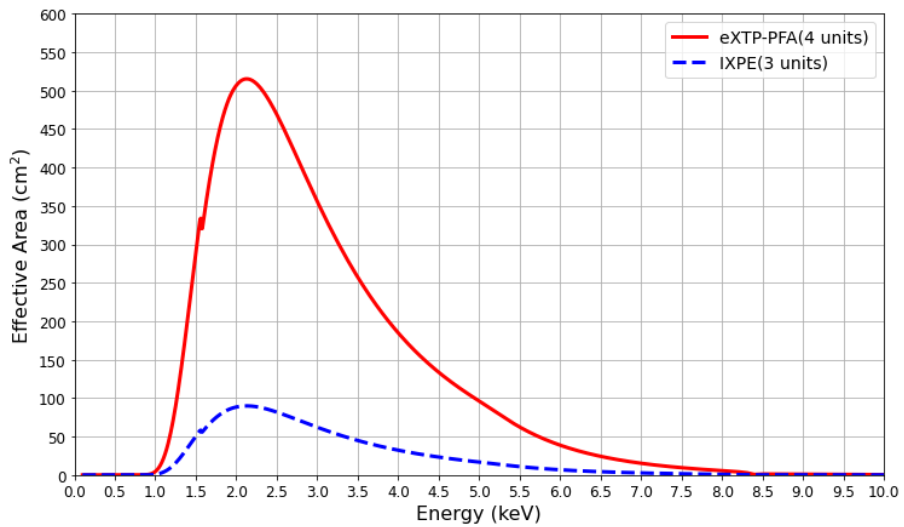Figure 19. Comparison of the total effective area between LAD and other collimated X-ray telescopes.

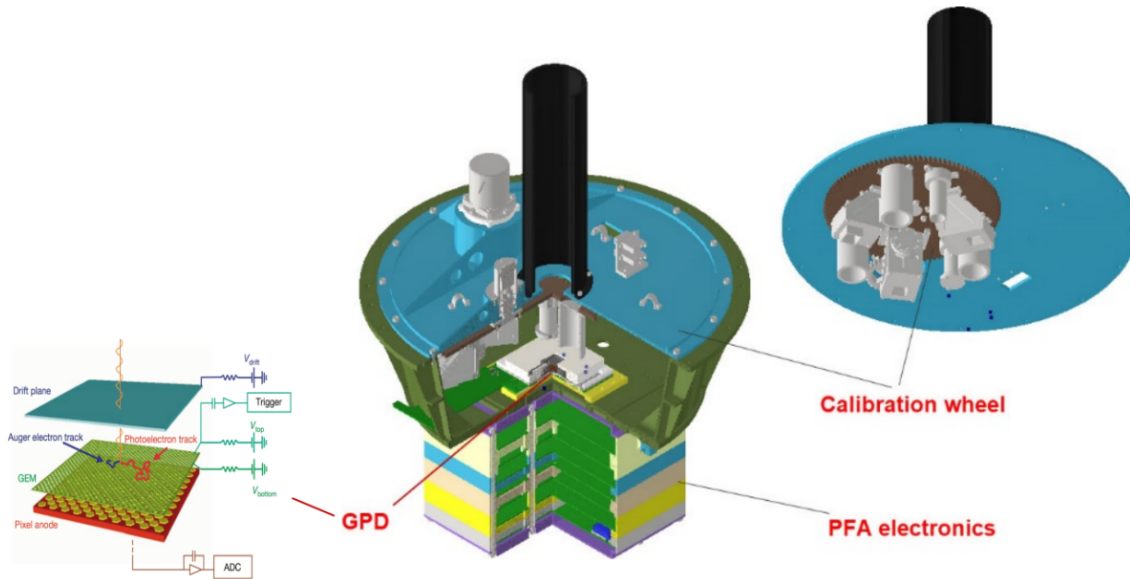Figure 20. Comparison of the total effective area between PFA and IXPE.

Figure 21. Focal plane camera of PFA.

unpolarized calibration sources, an opened aperture for week source observations, a gray filter for bright source observations, and a metal shutter on the filter wheel. The functions of the electronics box are data acquisition, scientific data packaging and transmission, command receiving and execution, housekeeping, GPD high voltage bias supply, GPD active thermal control, and secondary power supply. Scientific data are directly sent to the satellite platform through an LVDS interface of 80 Mbps, and low-speed instruction and data communication are realized through an instrument control unit, which services as the low-speed instruction and data communication router and the payload supply distribution switch array. All the telescopes in PFA and SFA share two instrument control units.

3.4 Wide Field Monitor (WFM)

The WFM consists of 6 wide field of view coded mask cameras, equipped with position sensitive detectors and arranged in three camera pairs (see Figure 14). Each camera has an effective field of view of 30° (fully coded) and 90° at zero response. The camera pairs axis are separated by ±60° around the line of sight of the Narrow Field of View Instruments (SFA, LAD and PFA), thus covering π sr = 3.1 sr (goal 4/3 π = 1.33 π = 4.1 sr, ~33% of the sky) and operating in the energy range 2-50 keV.

The main task of the WFM is to conduct long-term monitoring of targets of interest, and trigger and localize transient events (such as Gamma-Ray Bursts). WFM can provide important information of transient sources for the main telescope arrays, and decide whether to maneuver the platform to perform follow-up observations to transients according to pre-determined strategies. The comparison of the field of view between WFM and other wide field monitors can be seen in Figure 22. The details of the WFM design can refer to Ref. 31–35 and the references therein.

4. PROPOSED MISSION CONFIGURATION AND PROFILE

4.1 Mission Overview

According to the Space Science Programs of China, the eXTP mission consists of six systems. These are satellite system, launcher system, launch site system, TT&C system, ground support system, and science application system. The overall eXTP mission will be designed and implemented under China's responsibility with major contributions from the European Consortium. The system architecture and system level product tree are shown
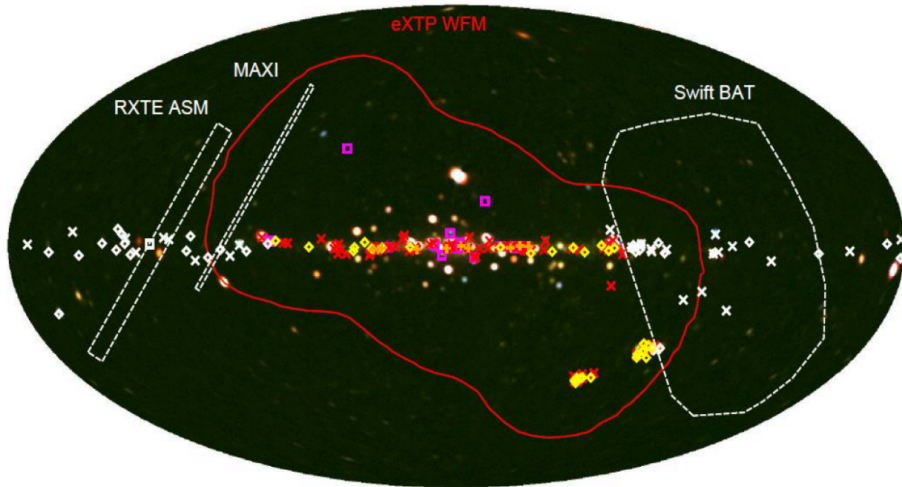
Figure 22. Comparison of the field of view between WFM and other field monitors.
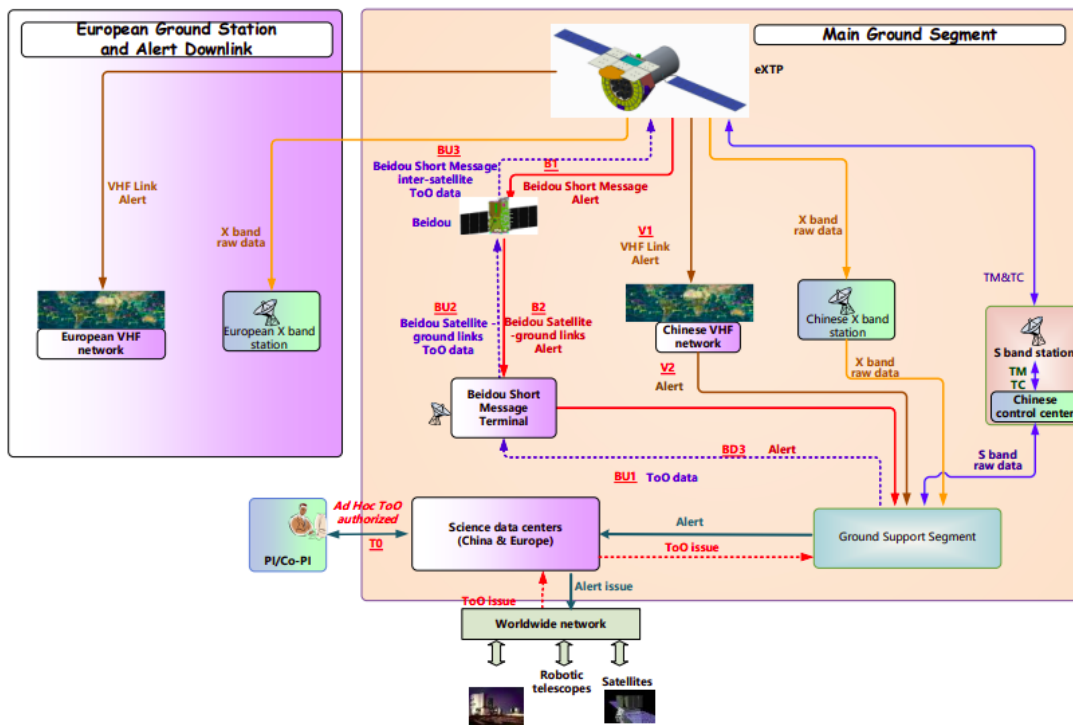

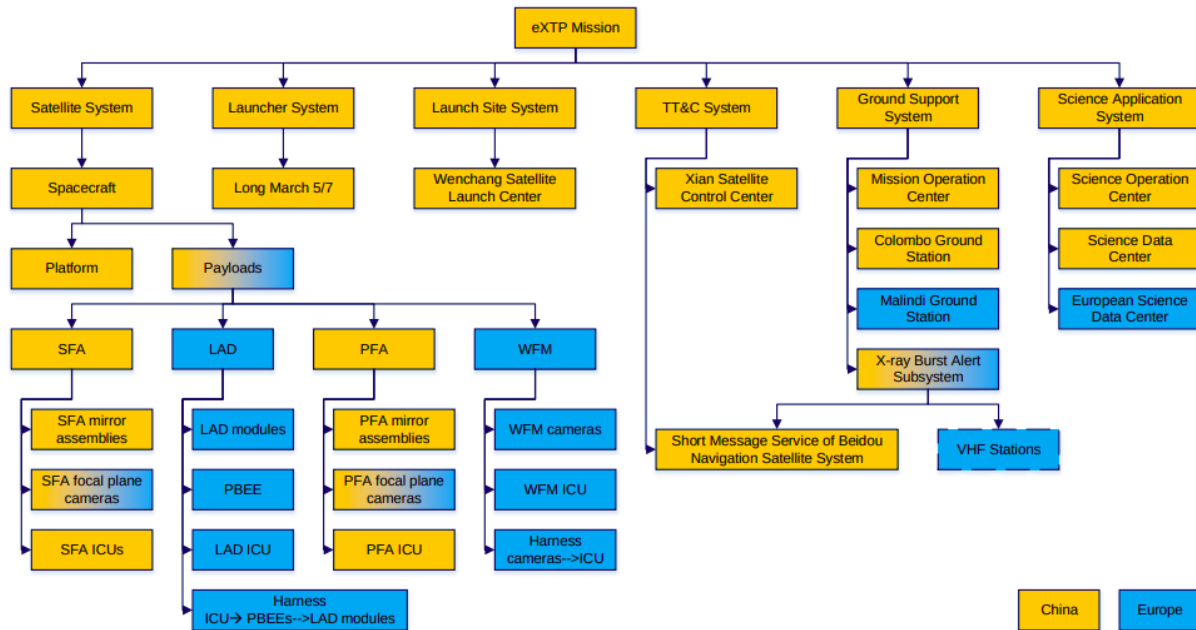
Figure 23. eXTP system architecture.

Figure 24. eXTP mission system-level product tree.

in Figure 23 and Figure 24, respectively. China will be in charge of the platform and satellite Assembling, Integration, and Testing (AIT), as well as the launch. The ground segment, operations, and data center infrastructure of the mission will be jointly organized by CAS and several European institutions and agencies.

The eXTP satellite will consist of a Chinese platform supporting the eXTP payloads. The Chinese side will provide the Spectroscopy Focusing Array (SFA) and the Polarimetry Focusing Array (PFA). The European side will provide the Large Area Detector (LAD) and the Wide Field Monitor (WFM).

In order to ensure the energy resolution of LAD and minimize the particle background of the payload, the orbit is selected as a 550 km circular orbit with an inclination angle of <2.5°. The three Narrow Field Instruments (NFIs: SFA, LAD and PFA) are installed coaxially to observe a target source, and WFM monitors sources in its very large FoV.

The satellite will be launched from the Wenchang launch site using CZ-5, to make direct entry into its orbit. The satellite carries propellant for orbit maintenance during the mission and also reserves enough propellant for de-orbit.

In order to meet the observational requirements, there are three types of communication links between the satellite and the ground station, i.e., S-band data link, X-band data link, Beidou short message link and VHF stations (a heritage from the China-France SVOM mission to be launched in 2023). S-band is used for satellite telemetry, tracking, and command (TT&C), X-band for scientific data down transmission, and Beidou short message link for the rapid uplink of ToO observation tasks. Both Beidou and VHF networks will be used for real-time downlink of WFM burst information.

The ground segment of eXTP consists of ground support system (including mission operation center, ground stations, and burst alert subsystem) and science application system (including science operation center and China/Europe science data center), as shown in Figure 23. The ground control center is responsible for satellite platform maintenance, platform observation planning and s-band telemetry data reception, etc. The science data center is responsible for observation execution, X-band data receiving, and long-term data archiving and storage. Considering the near-equatorial orbit, ground stations close to the equator are provided by China and European partners. The science data center is responsible for observation planning, scientific data processing, trigger information processing and distribution, and target of opportunity observation planning, etc.
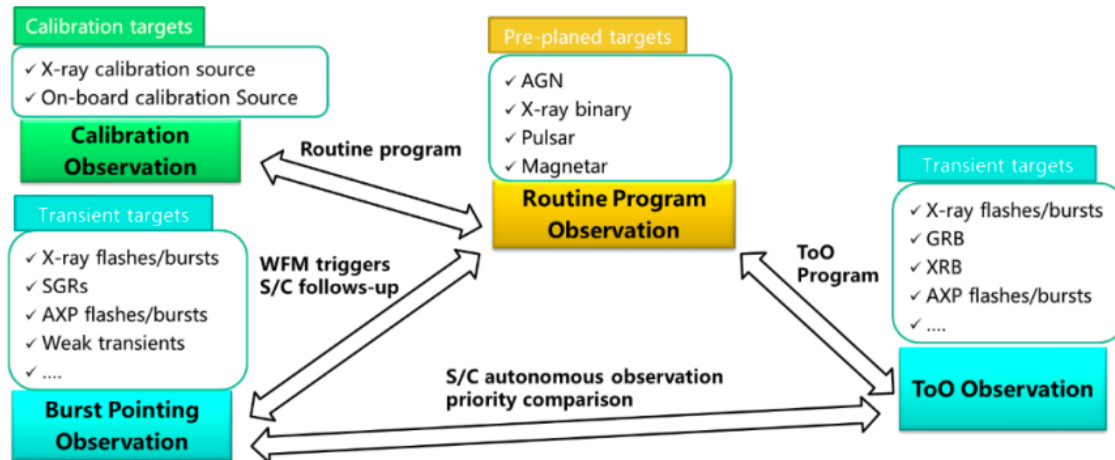
Figure 25. eXTP observation mode.

4.2 Observation Concept

4.2.1 Observation Mode

eXTP satellite is mainly used to observe celestial bodies in inertial space and maintaining triaxial stability. According to the requirements of scientific observation and on-orbit calibration, the satellite observation modes mainly include routine observation, follow up observation, target of opportunity (ToO), and small-sky scanning modes, as shown in Figure 25.

1. Routine observation mode: observations according to pre-planned observation targets.

2. Follow-up observation mode: dedicated to bursting source afterglow initial observation, consisting of an autonomous pointing towards the burst after the trigger and autonomous return to the current pointing. The autonomous point is a key requirement, which has been implemented in the satellite design. The WFM trigger information should be downloaded to ground in 30 s.

3. ToO observation mode: including observations programmed by the ground segment by ToO observing requests for astronomical events, additional calibrations, with time delay constraints. The observation plan should be uploaded in a few minutes.

4. Small sky scan mode: for PSF or vignetting function calibration of SFA, LAD and PFA, by scanning an X-ray source with ± 2 degree usually.

4.2.2 Pointing Strategy

According to the payload constraints on safety and thermal control, the pointing strategy of the satellite is as follows (see Figure 26):

1. The angle between the Sun and + Xsat should be >60°, to avoid stay light and thermal disturbance of all instruments.

2. The angle between the Sun and + Xsat should be <120°, to achieve stable thermal environment for LAD (180°, for observations without strict energy resolution requirement).

3. The Sun should be kept in the XoZ plane towards +Zsat. The angle between the Sun and the XoZ plane should be within ± 2°.
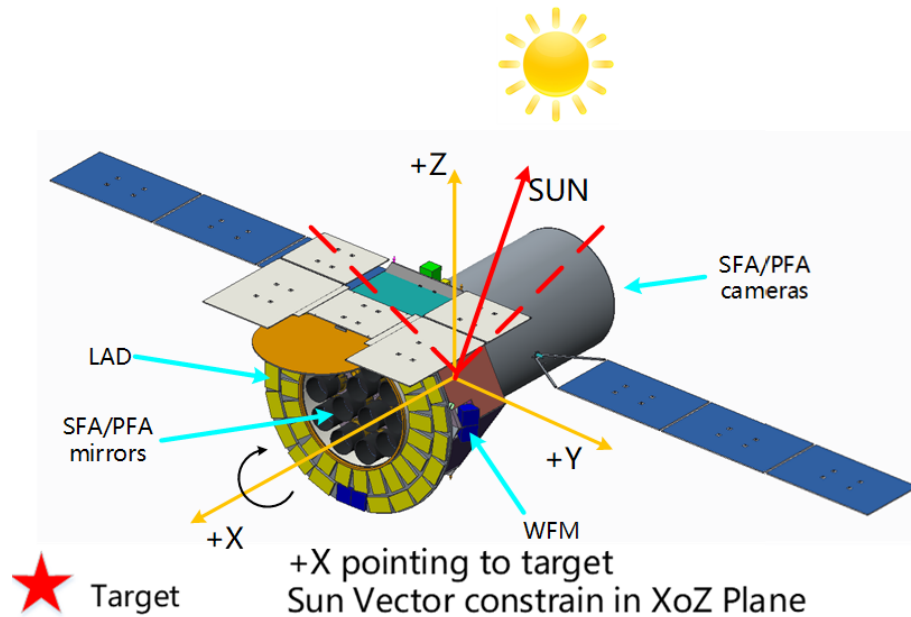
Figure 26. eXTP pointing strategy.

4.2.3 Pointing Performance Requirements

The principal axis of the satellite attitude pointing is defined as the star-tracker (STR) optical axis, i.e., STR-line-of-sight (STRLoS). When the satellite attitude control system uses STRLoS as the guidance axis, the optical axis of each payload should be parallel to the STRLoS to ensure that the payload can meet the imaging, effective area and other requirements.

Table 3. Pointing performance requirements.

Parameters	Requirements
Off-axis angle	SFA/PFA ±41"; LAD ±2.35'; WFM Calibrated
Detector axial deviation	SFA/PFA ±1 mm
Detector radial deviation	SFA/PFA ±0.5 mm
AOCS Absolute Knowledge Error (AKE)	1"
AOCS Absolute Pointing Error (APE)	3"
AOCS Relative Pointing Error (RPE)	Noise RMS caused by attitude jitter in frequency domain, see Figure 27
AOCS maneuver	30° in 10 mins

4.2.4 Target Visibility Analysis

The sky visibility (exposure time per year) is shown in Figure 28. The influences of the Earth and the Sun are considered in the estimation.

4.2.5 Mission Phases

eXTP operations are planned for 5 years, but the mission could be extended to an additional period of 3 years or any additional period that may be agreed by the participating parties. The mission operation is divided into 5 phases, the objectives of each phase being as follows:
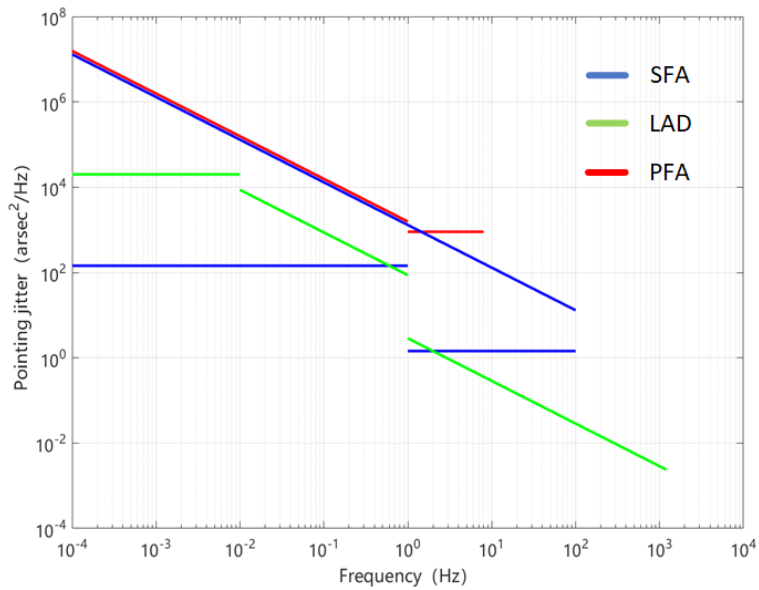
Figure 27. Payloads response stability requirements. It shows that the stability requirements below about 1 Hz is driven by SFA, while above about 1 Hz it is driven by LAD.
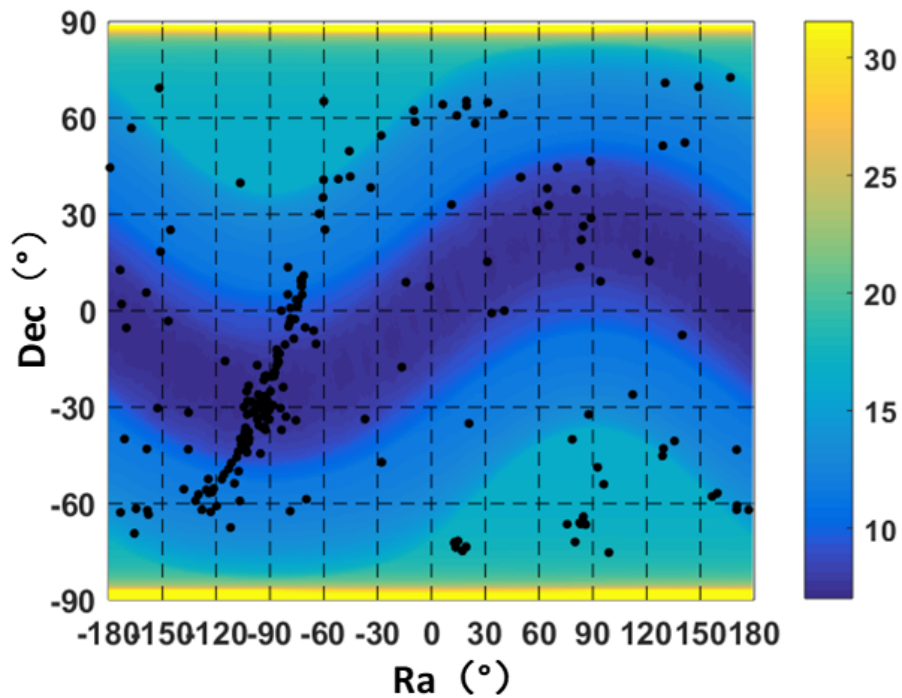

Figure 28. Observational visibility (Ms) per year with the consideration of the Sun and Earth constraints. The black dots are the potential targets of eXTP.

1. Launch and Early Orbit Phase (LEOP). The satellite is launched and maneuvered into its operational orbit. Satellite and instrument systems are activated and checked out.

2. Commissioning Phase. This phase begins at the end of LEOP and lasts up to 3 months.

3. Nominal Operations Phase. 5 years, normal mission phase for implementation of science observation plan, to reach the core and main scientific objectives.

4. Extended Operations Phase. Assuming useful data are still being collected, this phase extends the mission an additional 3 years or any additional period that may be agreed by the participating parties.

5. Decommissioning Phase. A controlled re-entry will be carried out to comply with casualty-risk regulations.

4.2.6 Science Exploitation and Policy

The observational program of eXTP is divided in a core program and a guest observer (GO) program. As shown in the Science Requirement document, ∼50% of the observing time is needed to reach the core objectives, so during the nominal mission phase (5 years) ∼50% observing time will be devoted to the GO program and to the Director Discretionary Time (DDT), the latter will be primarily used to respond to unanticipated or ad hoc ToOs. Both GO and DDT observations will be open to the whole international community. After this phase, the full (or most) observing time will be devoted to GO and DDT. Data relative to transient information like alert information regarding transient/outburst sources generated from WFM data, will be released immediately. SFA/LAD/PFA observational data will be released when the data proprietary period (one year, tentative) expires; however, all data from DDT observations will be released immediately. Scientific products/results obtained from data accumulation over years of mission operation will be published as scientific papers and/or data base when appropriate. These include, e.g. variable and transient source catalogs, the long-term light curves and spectral variations of monitored sources.

4.3 Satellite Design

In the design of satellite, a "centralized around payload" concept is adopted (see Figure 14 and Figure 29), which takes the payloads as the center of satellite and the platform units installed around the payloads. The central carbon-fiber reinforced plastics (CFRP) cylinders are to support the mirrors and cameras, and the platform units are installed on the panels around the central cylinder. The satellite is composed of 3 modules: the optical module (OM), platform module (PM) and detector module (DM). The observation direction is +X direction, the incident Sunlight is from +Z direction, and the Y axis is determined by right-hand rule. In order to provide the optimal mechanical environment for the payloads and ensure the accuracy, the LAD modules, WFM cameras and the mirror assemblies of SFA and PFA are accommodated on the +X side of the satellite. The cameras of SFA and PFA are placed on the -X side of the satellite which is 5250 mm away from the mirror assemblies. The 40 LAD modules are installed on the annular frame integrated with the main structure of the OM, and surround the mirror assemblies of SFA and PFA. The 6 WFM cameras are installed in pairs on the annular frame of LAD modules near the +X side of the satellite and ±Y side of PM respectively.

The satellite adopts a three-axis stable zero-momentum attitude control method, and has pointing modes such as inertial pointing, sun pointing and attitude maneuver. It carries 8 reaction wheels as the main actuators for attitude maneuvering to meet the requirements of 30° repointing within 600 s. When performing high-precision inertial pointing, the combination of high-precision star tracker, high-precision gyro and reaction wheels is used for attitude control. With four 10 N thrusters, the satellite has the capabilities of orbital maneuvering at the initial stage of orbit, orbit maintenance and debris avoidance during its 8-year lifetime in orbit. eXTP adopts the combined power supply scheme of solar cell array and battery pack. The solar cell array is installed in the ±Y direction of the satellite, the patch area is not less than 27.2 m^2, and a 300 Ah lithium-ion battery pack is used to meet the requirements of the whole satellite in the launch section and safety mode. Mature unified S-band (USB) transceiver is used for TT&C. The X-band is used for science data telemetry with transmission rate of 210 Mbps. A 5-Tbits solid-state memory is equipped for payload data storage. According to the thermal control requirements of the payload and the thermal environment of the orbit, a special design is carried out, and the combination of active thermal control and passive thermal control is used to meet the thermal control requirements of the satellite.
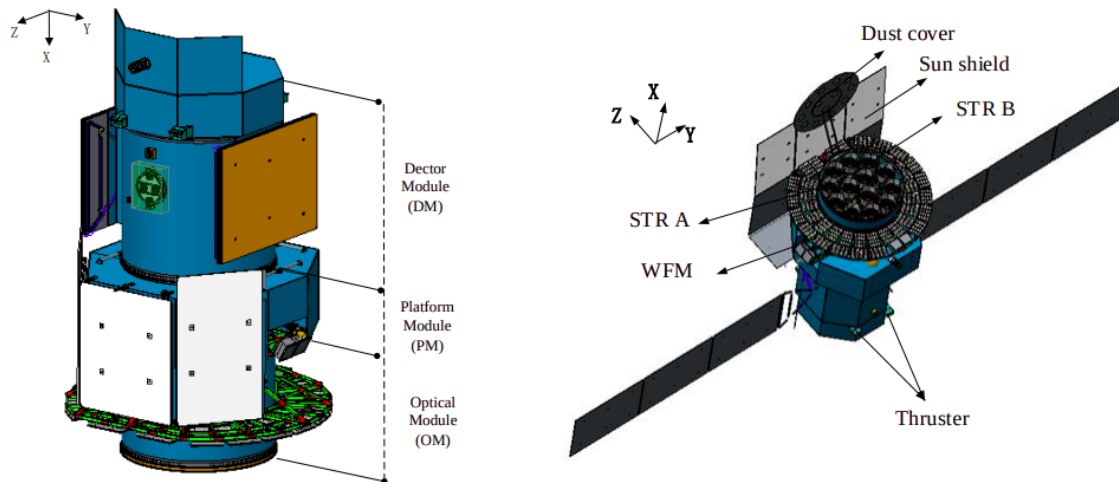
Figure 29. The launch and in-flight configuration.

5. SUMMARY

The enhanced X-ray Timing and Polarimetry mission (eXTP) is a flagship observatory for X-ray timing, spectroscopy and polarimetry developed by an International Consortium led by the Institute of High Energy Physics of the Chinese Academy of Science. The current baseline of the scientific payload includes four science instruments: the Spectroscopy Focusing Array (SFA), the Large Area Detector (LAD), the Polarimetry Focusing Array (PFA), and the Wide Field Monitor (WFM). Thanks to its very large collecting area, good spectral resolution and unprecedented polarimetry capabilities, eXTP will explore the properties of matter and the propagation of light in the most extreme conditions found in the Universe. eXTP will investigate three fundamental science areas: the equation of state of ultra-dense matter, the effects of strong-field gravity, the astrophysics and physics of very strong magnetic fields. eXTP will, in addition, be a powerful X-ray observatory. The mission will continuously monitor the X-ray sky,characterizing the active X-ray Universe on a large range of time scales, and will enable multi-wavelength and multi-messenger studies for gravitational waves and neutrinos sources.

The mission is proposed to be launched in a low-earth orbit at an altitude of ≤570 km. The inclination of the orbit is ≤2.5 deg. Nominal science operations will last for 5 years, with a design goal for 8-10 years. eXTP observations will comprise standard (planned) pointing observations, as well as targets of opportunity (ToO) triggered by WFM or other astrophysical facilities. A substantial fraction of its observation time will also be devoted to observatory science, through a fully open Guest Observer (GO) programme, and to coordinated multi-messenger programmes. The eXTP phase A studies were successfully concluded, and the mission is currently in phase B, which will be completed by the end of 2022. The launch of eXTP is planned for 2027.

ACKNOWLEDGMENTS

REFERENCES

[1] Zhang, S., Santangelo, A., Feroci, M., Xu, Y., Lu, F., Chen, Y., Feng, H., Zhang, S., Brandt, S., Hernanz, M., et al., "The enhanced x-ray timing and polarimetry mission—extp," *SCIENCE CHINA Physics, Mechanics & Astronomy* **62**(2), 1–25 (2019).

[2] Watts, A. L., Yu, W., Poutanen, J., Zhang, S., Bhattacharyya, S., Bogdanov, S., Ji, L., Patruno, A., Riley, T. E., Bakala, P., et al., "Dense matter with extp," *Science China Physics, Mechanics & Astronomy* **62**(2), 1–17 (2019).

[3] Lattimer, J. M. and Prakash, M., "The equation of state of hot, dense matter and neutron stars," *Physics Reports* **621**, 127–164 (2016).

[4] Baym, G., Hatsuda, T., Kojo, T., Powell, P. D., Song, Y., and Takatsuka, T., "From hadrons to quarks in neutron stars: a review," *Reports on Progress in Physics* **81**(5), 056902 (2018).

[5] Watts, A. L., Andersson, N., Chakrabarty, D., Feroci, M., Hebeler, K., Israel, G., Lamb, F. K., Miller, M. C., Morsink, S., Özel, F., et al., "Colloquium: Measuring the neutron star equation of state using x-ray timing," *Reviews of Modern Physics* **88**(2), 021001 (2016).

[6] Akmal, A. and Pandharipande, V. R., "Spin-isospin structure and pion condensation in nucleon matter," *Physical Review C* **56**(4), 2261 (1997).

[7] Li, A., Zhang, B., Zhang, N.-B., Gao, H., Qi, B., and Liu, T., "Internal x-ray plateau in short grbs: Signature of supramassive fast-rotating quark stars?," *Physical Review D* **94**(8), 083010 (2016).

[8] Bhattacharyya, S., Bombaci, I., Logoteta, D., and Thampan, A. V., "Fast spinning strange stars: possible ways to constrain interacting quark matter parameters," *Monthly Notices of the Royal Astronomical Society* **457**(3), 3101–3114 (2016).

[9] Zdunik, J. and Haensel, P., "Maximum mass of neutron stars and strange neutron-star cores," *Astronomy & Astrophysics* **551**, A61 (2013).

[10] Bednarek, I., Haensel, P., Zdunik, J., Bejger, M., and Mańka, R., "Hyperons in neutron-star cores and a 2 $m_\odot$ pulsar," *Astronomy & Astrophysics* **543**, A157 (2012).

[11] Hebeler, K., Lattimer, J., Pethick, C. J., and Schwenk, A., "Equation of state and neutron star properties constrained by nuclear physics and observation," *The Astrophysical Journal* **773**(1), 11 (2013).

[12] Kurkela, A., Fraga, E. S., Schaffner-Bielich, J., and Vuorinen, A., "Constraining neutron star matter with quantum chromodynamics," *The Astrophysical Journal* **789**(2), 127 (2014).

[13] Nättilä, J. and Pihajoki, P., "Radiation from rapidly rotating oblate neutron stars," *Astronomy & Astrophysics* **615**, A50 (2018).

[14] Riley, T. E., Watts, A. L., Ray, P. S., Bogdanov, S., Guillot, S., Morsink, S. M., Bilous, A. V., Arzoumanian, Z., Choudhury, D., Deneva, J. S., et al., "A nicer view of the massive pulsar psr j0740+ 6620 informed by radio timing and xmm-newton spectroscopy," *The Astrophysical Journal Letters* **918**(2), L27 (2021).

[15] Miller, M., Lamb, F., Dittmann, A., Bogdanov, S., Arzoumanian, Z., Gendreau, K., Guillot, S., Ho, W., Lattimer, J., Loewenstein, M., et al., "The radius of psr j0740+ 6620 from nicer and xmm-newton data," *The Astrophysical Journal Letters* **918**(2), L28 (2021).

[16] Salmi, T., Loktev, V., Korsman, K., Baldini, L., Tsygankov, S. S., and Poutanen, J., "Neutron star parameter constraints for accretion-powered millisecond pulsars from the simulated ixpe data," *Astronomy & Astrophysics* **646**, A23 (2021).

[17] Viironen, K. and Poutanen, J., "Light curves and polarization of accretion-and nuclear-powered millisecond pulsars," *Astronomy & Astrophysics* **426**(3), 985–997 (2004).

[18] Bardeen, J. M., Press, W. H., and Teukolsky, S. A., "Rotating black holes: locally nonrotating frames, energy extraction, and scalar synchrotron radiation," *The Astrophysical Journal* **178**, 347–370 (1972).

[19] Raaijmakers, G., Greif, S., Hebeler, K., Hinderer, T., Nissanke, S., Schwenk, A., Riley, T., Watts, A., Lattimer, J., and Ho, W., "Constraints on the dense matter equation of state and neutron star properties from nicer's mass–radius estimate of psr j0740+ 6620 and multimessenger observations," *The Astrophysical Journal Letters* **918**(2), L29 (2021).

[20] Adhikari, P., Andersen, J. O., and Mojahed, M. A., "Quark, pion and axial condensates in three-flavor finite isospin chiral perturbation theory," *The European Physical Journal C* **81**(5), 1–12 (2021).

[21] Reynolds, C. S., "Observational constraints on black hole spin," *Annual Review of Astronomy and Astrophysics* **59**(1), 117–154 (2021).

[22] Miller, J., Miller, M., and Reynolds, C., "The angular momenta of neutron stars and black holes as a window on supernovae," *The Astrophysical Journal Letters* **731**(1), L5 (2011).

[23] Rosa, A. D., Uttley, P., Gou, L., Liu, Y., Bambi, C., Barret, D., Belloni, T., Berti, E., Bianchi, S., Caiazzo, I., et al., "Accretion in strong field gravity with extp," *SCIENCE CHINA Physics, Mechanics & Astronomy* **62**(2), 1–29 (2019).

[24] Maccarone, T. J. and Schnittman, J. D., "The bicoherence as a diagnostic for models of high-frequency quasi-periodic oscillations," *Monthly Notices of the Royal Astronomical Society* **357**(1), 12–16 (2005).

[25] Santangelo, A., Zane, S., Feng, H., Xu, R., Doroshenko, V., Bozzo, E., Caiazzo, I., Zelati, F. C., Esposito, P., Gonzalez-Caniulef, D., et al., "Physics and astrophysics of strong magnetic field systems with extp," *SCIENCE CHINA Physics, Mechanics & Astronomy* **62**(2), 1–23 (2019).

[26] in 't Zand, J. J. M., Bozzo, E., Qu, J., Li, X.-D., Amati, L., Chen, Y., Donnarumma, I., Doroshenko, V., Drake, S. A., Hernanz, M., et al., "Observatory science with extp," *Science China Physics, Mechanics & Astronomy* **62**, 29506 (Aug 2018).

[27] Abbott, B. P., Abbott, R., Abbott, T., Acernese, F., Ackley, K., Adams, C., Adams, T., Addesso, P., Adhikari, R., Adya, V. B., et al., "Gw170817: observation of gravitational waves from a binary neutron star inspiral," *Physical review letters* **119**(16), 161101 (2017).

[28] Abbott, B. P., Abbott, R., Abbott, T., Acernese, F., Ackley, K., Adams, C., Adams, T., Addesso, P., Adhikari, R., Adya, V., et al., "Gravitational waves and gamma-rays from a binary neutron star merger: Gw170817 and grb 170817a," *The Astrophysical Journal Letters* **848**(2), L13 (2017).

[29] Stratta, G. and Santangelo, A., "X- and Gamma-ray astrophysics in the era of Multi-messenger astronomy," (5 2022). (Handbook of X-ray and Gamma-ray Astrophysics, chief eds C. Bambi and A. Santangelo, Springer).

[30] Feroci, M., Ambrosi, G., Ambrosino, F., Antonelli, M., Argan, A., Babinec, V., Barbera, M., Bayer, J., Bellutti, P., et al., "The Large Area Detector onboard the eXTP mission," International Society for Optics and Photonics, SPIE (2022). (In press, in the same volume).

[31] Xiong, H., Argan, A., Baudin, D., Bayer, J., Bouyjou, F., Monte, E. D., Evangelista, Y., Feroci, M., Gálvez, J.-L., Hedderman, P., et al., "The digital data processing concepts of the Large Area Detector and the Wide Field Monitor onboard eXTP," International Society for Optics and Photonics, SPIE (2022). (in press, in the same volume).

[32] Hernanz, M., Brandt, S., in 't Zand, J., Evangelista, Y., Meuris, A., Tenzer, C., Zampa, G., Orleanski, P., Kalemci, E., Schanne, S., , et al., "The Wide Field Monitor onboard the Chinese-European X-ray mission eXTP," International Society for Optics and Photonics, SPIE (2022). (in press, in the same volume).

[33] Zwart, F., Tacken, R., in 't Zand, J., de la Rie, R., Limpens, M., Kochanowski, C., Aitink-Kroes, G., van Baren, C., Bayer, J., Baudin, D., et al., "The detector/readout-electronics assembly of the eXTP Wide Field Monitor," International Society for Optics and Photonics, SPIE (2022). (in press, in the same volume).

[34] Kalemci, E., Turhanb, O., Kuvvetli, I., Schanne, S., Hernanz, M., Orleanski, P., Tenzer, C., Süngur, M., Onath, A., Bozkurt, A., Baltacı, M. A., Gálvez, J.-L., Brandt, S., Skup, K., Tcherniak, D., and Michalska, M., "The Instrument Control Unit processing hardware and the software of the Wide Field Monitor on eXTP," International Society for Optics and Photonics, SPIE (2022). (in press, in the same volume).

[35] Gálvez, J.-L., Hormaetxe, A., Hernanz, M., Ferrés, P., Taubmann, G., Casalta, J. M., and Tomás, A., "The mechanical design and implementation of the WFM cameras for eXTP," International Society for Optics and Photonics, SPIE (2022). (in press, in the same volume).